Integrated multi-omics reveals coordinated *Staphylococcus aureus* metabolic, iron transport, and stress responses to human serum

Warasinee Mujchariyakul[1], Calum J. Walsh[1,2], Stefano Giulieri[1,2,3], Kim-Ahn LêCao[4], Timothy P. Stinear[1,2], Benjamin P. Howden[1,2,5*], Romain Guérillot[1,2*] and Abderrahman Hachani[1,2*]

Author addresses:

[1] Department of Microbiology and Immunology, The University of Melbourne at the Peter Doherty Institute for Infection and Immunity, Melbourne, Victoria, Australia.

[2] Centre for Pathogen Genomics, The University of Melbourne, Melbourne, Victoria, Australia.

[3] Victorian Infectious Diseases Service, Royal Melbourne Hospital, The Peter Doherty Institute for Infection and Immunity, Melbourne, Victoria, Australia

[4] Melbourne Integrative Genomics, School of Mathematics and Statistics, University of Melbourne, Melbourne, Victoria, 3000, Australia.

[5] Microbiological Diagnostic Unit Public Health Laboratory, Department of Microbiology and Immunology, Doherty Institute, University of Melbourne, Melbourne, Victoria, Australia.

* Joint senior authors

Keywords: *Staphylococcus aureus*, Multi-omics data integration, Metabolism, iron acquisition, stress responses, bacteraemia

Running title: ***Staphylococcus aureus* adaptive responses to human serum**

ABSTRACT

Bloodstream infections caused by *Staphylococcus aureus* remain a leading cause of mortality worldwide. Our understanding of *S. aureus* survival and persistence in human serum, a cell-free fraction of blood hostile for bacteria, is still limited. Here, we applied multivariate data integration methods and network analysis to a multi-omic dataset generated from five clinically prevalent *S. aureus* genotypes exposed to human serum. We observed and then confirmed using isogenic mutants, the significant roles of *gapdhB*, *sucA*, *sirA*, *sstD*, and *perR* in bacterial survival in serum. These data show that metabolic versatility in carbon source usage, iron transport and resistance to oxidative stress are interlinked and central to *S. aureus* fitness in serum, representing potential *S. aureus* vulnerabilities that could be exploited therapeutically.

IMPORTANCE

Bloodstream infections caused by *Staphylococcus aureus* are associated with mortality rates of up to 30%. However, the molecular mechanisms that enable this pathogen to survive in human serum, a nutrient-limited and immunologically hostile environment remain poorly understood. By integrating multi-omic data from five clinically relevant *S. aureus* genotypes and validating key signatures using mutants, we identified conserved genetic determinants critical for bacterial survival in serum. Our findings highlight the interconnected roles of carbohydrate metabolic flexibility, iron acquisition, and oxidative stress resistance in shaping *S. aureus* adaptation to serum. This work advances our understanding of microbial strategies to survive in the bloodstream and demonstrate the potential of multi-omic integration to uncover therapeutic vulnerabilities in bacterial pathogens.

52 **INTRODUCTION**

53 *Staphylococcus aureus* is a significant opportunistic human pathogen (Howden et al., 2023). As a
54 commensal, *S. aureus* coexists with other members of the human microbiome in up to 30% of the
55 human population, typically colonizing the skin or nares, with the potential to become a lethal
56 pathogen (Räz et al., 2023). *S. aureus* bloodstream infections are greater than 10 in 100,000 people
57 per year, with the severity of infections compounded by the widespread emergence of resistance to
58 last-line antibiotics such as vancomycin, and mortality rates reaching 20% (Murray et al., 2022).

59 During bloodstream infections, professional phagocytes and non-cellular immune components,
60 including antimicrobial peptides (AMPs), immunoglobulins and the complement system, target
61 invasive pathogens for clearance (Guerra et al., 2017; Hornef et al., 2002). While serum does not
62 contain immune cells, it represents a potent bactericidal environment for blood-invasive bacterial
63 pathogens (Kuehl et al., 2020; Lopatkin et al., 2019; Mathew et al., 2023); an environment against
64 which *S. aureus* has evolved multiple defence mechanisms (Howden et al., 2023; Kwiecinski &
65 Horswill, 2020; Price & Boyd, 2020). The bacterium can evade humoral immunity by directly
66 interfering with antibody functions to prevent opsonization for phagocytosis (Bear et al., 2023; de
67 Jong et al., 2019), or by degrading complement components (Paiva et al., 2023). *S. aureus* can
68 inactivate AMPs through proteolytic degradation (Joo & Otto, 2015), modification of its surface
69 charge, or remodelling both the organization of its cell wall peptidoglycan and the abundance of
70 cardiolipin in its plasma membrane. The latter two processes also contribute to *S. aureus* resistance
71 to cell wall-targeting antibiotics (Ledger et al., 2022). The host can also impose nutritional immunity
72 by sequestering essential nutrients, primarily trace metals like iron, zinc, and manganese to restrict
73 bacterial growth. Bacterial pathogens have evolved mechanisms to circumvent nutritional immunity
74 (Murdoch & Skaar, 2022). For example, *S. aureus* has multiple trace metal-sequestering strategies
75 that also contribute to its survival in blood (Cassat & Skaar, 2012).

76 Elucidating the metabolic reprogramming of *S. aureus* in response to serum-derived stressors—such
77 as nutrient limitation and acellular immune factors—can uncover fundamental metabolic pathways

that facilitate its adaptation, survival, and persistence in the bloodstream. These insights may inform the development of targeted antimicrobial strategies and rationally designed interventions to mitigate invasive and chronic *S. aureus* infections.

We previously reported a comprehensive multi-omics analysis of four clinically significant sepsis-causing bacterial pathogens (*Escherichia coli*, *Klebsiella pneumoniae, S. aureus*, and *Streptococcus pyogenes*) following their exposure to human serum (Mu et al., 2023). This work revealed a set of conserved adaptive responses across these phylogenetically diverse species.
Notably, all four pathogens exhibited a coordinated upregulation of lipid metabolic pathways that was associated with extensive remodelling of the cell envelope. This adaptation likely reflects a shared osmoprotective strategy, enhancing bacterial survival in the hostile and nutrient-limited environment of human serum. Building on our multi-omics dataset, this study examines the serum response of *Staphylococcus aureus* across five clinically relevant clonal lineages—BPH2760 (ST1), BPH2819 (ST5), BPH2900 (ST22), BPH2947 (ST239), and BPH2986 (ST8). The aim is to identify a conserved set of molecular features that drives species-specific adaptation to serum during septicaemia.

With a focused analysis on *S. aureus*, we refined here our analytical workflow. In our previous study (Mu et al., 2023), we used a late-integration approach, independently analysing transcriptomic, proteomic, and metabolomic datasets before mapping significant features to metabolic pathways and Gene Ontology terms. While this revealed broad functional patterns, it lacked the resolution to detect coordinated molecular changes across omics layers or to uncover direct cross-omic relationships. To address these limitations, we adopted the DIABLO framework (Data Integration Analysis for Biomarker discovery using Latent cOmponents) from the mixOmics R package, which applies a sparse, multiblock partial least squares (PLS) method, optimised to integrate all omics datasets within a single multivariate model. By selecting a minimal set of features that co-vary across data types and

103 distinguish between serum- and RPMI-exposed conditions, DIABLO enables the identification of
104 cross-omic interactions, reduces the statistical burden of separate analyses, and preserves the
105 integrated biological context of the *S. aureus* serum response (Rohart et al., 2017; Singh et al., 2019).
106 We further interrogated these signatures using differential expression and network-based analyses,
107 and identified interconnected metabolic pathways involved in serum adaptation through over-
108 representation analysis (ORA) and Gene Set Enrichment Analysis (GSEA).
109 Our integrated omic analysis show that *S. aureus* maintains optimal fitness in serum by undergoing
110 changes in key carbohydrate metabolic processes, iron acquisition, and resistance to oxidative stress
111 pathways. This combined response likely enables *S. aureus* to withstand host stressors such as
112 nutritional immunity and promote its survival in human serum.
113
114

115 **RESULTS**

116 **Coordinated transcriptomic, proteomic, and metabolomic adaptation of *S. aureus* to serum**

117 We performed multi-omics analysis to find the shared molecular responses to human serum of five
118 *S. aureus* clinical isolates (BPH2760, BPH2819, BPH2900, BPH2947, and BPH2986) (**Figure 1A**).
119 Principal Component Analysis (PCA), a dimensionality reduction method, was applied to each omics
120 layer, revealing clear separation between serum- and RPMI-exposed *S. aureus*. In each omic dataset,
121 the first principal component explained approximately 30% of the total variance, capturing the
122 dominant condition-specific signal (**Figure 1B**). We used DIABLO to integrate the datasets into a
123 unified predictive model of *S. aureus* exposure to human serum. DIABLO is a supervised multiblock
124 method based on sparse Partial Least Squares Discriminant Analysis (sPLS-DA) (Rohart et al., 2017;
125 Singh et al., 2019). DIABLO enabled simultaneous feature selection (a 'feature' is defined here as a
126 molecular variable derived from transcriptomic, proteomic, or metabolomic datasets) and
127 identification of highly correlated molecular signatures that distinguished *S. aureus* responses to
128 serum versus the control condition (RPMI) (**Figure 1C-D**, **Figure S1A**). The sample plot showed
129 that the first component captured most of the common serum responses across all five *S.*
130 *aureus* strains, while the second component reflected strain-specific variation (**Figure S1B**). The final
131 DIABLO model used 60 multi-omic features (see methods) that optimally discriminated serum from
132 RPMI exposure on the first component (**Table S1**, **Figure S1C**).

133

134 A coordinated serum response signature was indicated by highly correlated latent components across
135 the omics layers, including transcriptomic, proteomic and metabolomic, (Pearson's $r > 0.95$), (**Figure**
136 **1C**). Loading values from the DIABLO model (**Figure 1D**) show the specific contribution of
137 individual variables, with higher absolute values marking greater discriminative power.

138

139 To explore consistent patterns between omics data, a similarity matrix was calculated across all
140 components and selected features (**Table S1**) and visualized as a network (**Figure 1E)** (González et

141 al., 2012). The network revealed interactions across transcriptomic, proteomic and metabolomic
142 layers, with features grouped by function and showing both positive and negative correlations and
143 suggesting a coordinated response to serum. The staphylococcal pathways enriched among the
144 discriminant and correlated features identified by DIABLO included cell wall biosynthesis,
145 carbohydrate metabolism, iron transport, and defence against host immunity (**Figure 1D, 1E and**
146 **Table 1)**. CDS and their products central to these pathways exhibited strong positive correlations: i)
147 *glmS*, pivotal in the cell wall biosynthesis and lipid metabolism (via linoleic and oleic acids, and
148 cholesterol metabolites); ii) *gapdhB* and *sucA*, involved in carbohydrate metabolism, and *sstD*, *scdA*,
149 and *isdB*, contributing to iron uptake; and iii) *perR* and *sbi*, supporting oxidative stress resistance
150 mechanisms and immune evasion, respectively. In contrast, genes involved in nucleotide metabolism
151 (*mtaB*, *miaB*, *guaC*) were negatively correlated with carbohydrate metabolism genes (*gapdhB* and
152 s*ucA*) and lipids (linoleic and oleic acids).
153
154 The observed patterns show that *S. aureus* undergoes substantial metabolic adaptation in response to
155 serum, engaging uptake and utilization of serum-derived amino acids, carbohydrates, fatty acids,
156 nucleotides, and their derivatives. Notably, the analysis revealed a marked increase in the abundance
157 of staphylococcal iron acquisition proteins upon serum exposure. In the host environment,
158 extracellular iron is limited and typically sequestered by high-affinity iron-binding proteins such as
159 transferrin, lactoferrin, and haemoglobin within erythrocytes. The elevated levels of both
160 siderophore-dependent (HtsA, SirA, SstA) and siderophore-independent (IsdB) iron acquisition
161 proteins underscore the critical role of iron sequestration in *S. aureus* survival (**Figure 1D**). The
162 integration of multi-omic data reveal the responses that support metabolic resilience, enabling *S.*
163 *aureus* to maintain fitness while countering intrinsic serum stressors.

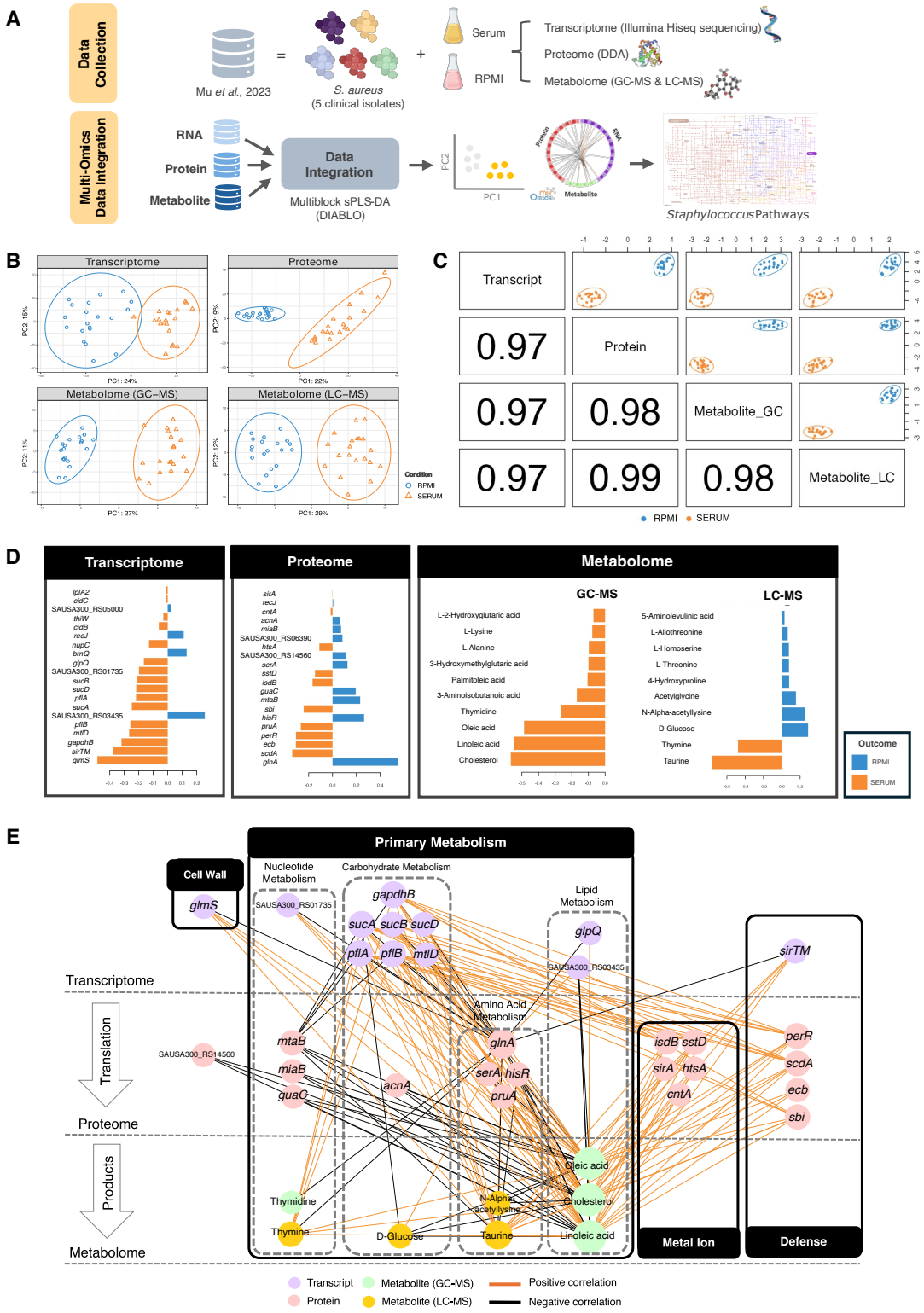

164

165 **Figure 1. Multi-omics identification of molecular signatures of *S. aureus* adaptation to serum**

166 (A) Schematic workflow of multi-omics analysis to predict *S. aureus* signature molecules in response

167 to human serum; (B) Unsupervised analysis using Principal Component Analysis (PCA). Sample plot

168 from PCA illustrating the consistency of sample clustering across datasets (transcriptomics,

169 proteomics, and metabolomics (GC-MS and LC-MS)), with samples labelled based on media
170 conditions (SERUM and RPMI); (C) Supervised analysis using multiblock sPLS-DA. Diagnostic plot
171 (sample scatter plot), according to media conditions (SERUM and RPMI). The numbers in each block
172 below the diagonal represent correlation coefficients between the first components of each dataset;
173 (D) Loading plot depicting features selected as optimally discriminatory between conditions by PLS-
174 DA from the first component in each dataset; (E) Correlation network visualizing pairwise
175 correlations (> |0.9|) between variables (transcripts, proteins, metabolites). Edge connections
176 represent correlations, with edge colors indicating positive (orange) or negative (black) correlations.
177 Node sizes are proportional to the number of interactions, and node colors represent data types: purple
178 (transcripts), pink (proteins), green (GC-MS metabolites), and yellow (LC-MS metabolites).
179
180 **Table 1.** Functions of selected variables shown in **Figure 1E**

Variable Name	Function	Reference
acnA/ citB (SAUSA300_RS06765)	TCA cycle	(Cox & Nelson, 2008)
Alpha/beta hydrolase (SAUSA300_RS03435)	Putative lipase/esterase Maintenance of bacterial homeostasis and mediation of host-pathogen interactions	(Fuchs et al., 2018; Simon & Cravatt, 2010)
cntA (SAUSA300_RS13350)	Transport of multiple metals such as nickel, cobalt, zinc, iron, copper, and manganese	(Ghssein et al., 2016; Grim et al., 2017; Remy et al., 2013)
ecb (SAUSA300_RS05670)	Complement binding	(Jongerius et al., 2010)
gapdhB (SAUSA300_RS08910)	Gluconeogenesis	(Purves et al., 2010)
glpQ (SAUSA300_RS04655)	Utilization of glycerophosphodiesters (GroPC, GroPI, GroPS, GroPE, and GroPG) and release of glycerol-3-phosphate	(Jorge et al., 2017)
glnA (SAUSA300_RS06485)	Synthesis of L-glutamine from L-glutamate	(Gustafson et al., 1994)
guaC (SAUSA300_RS06695)	Conversion of GMP to IMP	(Wolff et al., 2022)
hstA (SAUSA300_RS11760)	Substrate-binding protein in siderophore-dependent iron acquisition pathways	(Beasley, Marolda, et al., 2011)
Hypothetical protein/ hisR (SAUSA300_RS10330)	Repressor in Histidine biosynthesis	(Fuchs et al., 2018)
isdB (SAUSA300_RS05535)	Substrate-binding protein in siderophore-independent iron acquisition pathways (heme–iron uptake pathway), interaction with von Willebrand factor, promotion of adherence to endothelial cells	(Alfeo et al., 2021; Mathelié-Guinlet et al., 2020)
sbi (SAUSA300_RS13060)	Complement binding	(Burman et al., 2008)
scdA (SAUSA300_RS01350)	Repair of oxidative and nitrosative damage to iron-sulphur centres and role in cell wall metabolism	(Brunskill et al., 1997; Overton et al., 2008)
serA (SAUSA300_RS09115)	Biosynthesis of L-serine	(Zhang et al., 2017)
sirA (SAUSA300_RS00605)	Substrate-binding protein in siderophore-dependent iron acquisition pathways	(Beasley, Marolda, et al., 2011)
sirTM (SAUSA300_RS01740)	Regulation of oxidative stress	(Rack et al., 2015)
sucA (SAUSA300_RS07105)	TCA cycle	(Cox & Nelson, 2008)
sucB	TCA cycle	(Cox & Nelson, 2008)

(SAUSA300_RS07100)		
sucD (SAUSA300_RS06165)	TCA cycle	(Cox & Nelson, 2008)
sstD (SAUSA300_RS03880)	Substrate-binding protein in siderophore-dependent iron acquisition pathways	(Beasley, Marolda, et al., 2011)
miaB (SAUSA300_RS06405)	Modification of tRNA	(Arragain et al., 2010)
mtaB (SAUSA300_RS08375)	Modification of tRNA	(Arragain et al., 2010)
mtlD (SAUSA300_RS11620)	Conversion of mannitol-1-P to fructose-6-P	(Murphey & Rosenblum, 1964)
perR (SAUSA300_RS10060)	Sensing of Hydrogen Peroxide (H_2O_2)	(Ji et al., 2015)
pflA (SAUSA300_RS01160)	Role in Formate metabolism	(Leibig et al., 2011)
pflB (SAUSA300_RS01155)	Role in Formate metabolism and promotion of biofilm persistence	(Bertrand et al., 2022; Leibig et al., 2011)
Polyisoprenoid-binding protein (SAUSA300_RS14560)	Role in the electron transport system	(Handa et al., 2005; Wolff et al., 2022)
Protein-ADP-ribose hydrolase (SAUSA300_RS01735)	Reversal of ADP-ribosylation in posttranslational modification	(Rack et al., 2020)
pruA/rocA (SAUSA300_RS13840)	Catabolism of proline to glutamate	(Christgen & Becker, 2019)

Network and enrichment analyses reveal *S. aureus* shared and strain-specific responses to serum

Differentially expressed (DE) genes or proteins for each strain were identified and further subjected to an intersection analysis. This analysis showed that at the transcript level, 143 genes were up-regulated, and 65 genes were down-regulated in response to serum. At the proteomic level, there were 21 up-regulated and 17 down-regulated proteins in response to serum (**Figure S2A-B, Table S2**). We performed a Pathway Enrichment Analysis (PEA), including an overrepresentation analysis (ORA) and a gene set enrichment analysis (GSEA), to reduce the complexity of data and find overrepresented pathways elicited upon exposure to serum. ORA is widely used to identify over-represented biological functions in DE gene sets, performing best when handling wide gene expression differences. Genes were filtered using criteria of log2 fold change (log2FC) > 1 and adj-P value < 0.05. To improve the granularity of PEA outputs, a GSEA analysis was also applied to capture pathways where gene expression changes were more subtle but consistently enriched, enabling the detection of significant, but lower-magnitude responses. Using the similarity in gene subsets shared between pathways, we also conducted a network analysis to find interactions among the enriched

198 pathways across the omics layers (**Figure 2A, Figure S3A-J, Table S3**). Consistent with previous
199 DIABLO findings, ORA and GSEA identified four distinct functional modules comprising
200 carbohydrate metabolism, ribosome-associated pathways, iron acquisition, and nucleotide
201 metabolism (**Figure 2B-E**).
202
203 The carbohydrate metabolism module was composed of the glycolysis/gluconeogenesis pathway,
204 along with other carbohydrate-processing routes such as phosphotransferase systems (PTS) (**Figure**
205 **2B-C**). Upregulated carbohydrate transporter genes, *uhpT*, *mtlA*, *fruA*, *glcC*, *lacE*,
206 SAUSA300_RS01760, and *rbsU,* support the usage of various saccharides, including glucose,
207 fructose, lactose, D-mannitol, and ribose (**Table S2**). Once transported and phosphorylated by PTS,
208 carbohydrates such as glucose and fructose, are processed by glycolysis and converted into ribose-5-
209 phosphate, glyceraldehyde-3-phosphate, and fructose-6-phosphate intermediates. These key
210 metabolites bridge glycolysis to nucleotide and lipid metabolism (Kim et al., 2023; Richardson et al.,
211 2015) (further detailed in **Figure 4)**, thereby enhancing the staphylococcal metabolic flexibility in
212 serum. In contrast to other metabolic modules, our network analysis revealed that ribosome-
213 associated pathways were largely isolated, exhibiting no direct connectivity with broader metabolic
214 networks (**Figure 2C, Figure S3A-D**). Transcriptome profiling indicated a suppression of ribosome
215 biogenesis following serum exposure, characterized by the downregulation of genes encoding 30S
216 and 50S ribosomal subunit proteins (**Table S2 and S3)** Expression of the translational
217 GTPase *typA* (also known as *bipA*), a critical regulator of ribosome assembly and translational
218 fidelity under stress conditions (Gibbs et al., 2020; Njenga et al., 2023), was also significantly reduced
219 (**Table S2)**. These findings show that the protein biogenesis is downregulated as part of a stress-
220 adaptive response of *S. aureus* to serum.
221
222 Among the proteomic changes induced by serum exposure, iron acquisition and nucleotide
223 metabolism pathways showed the most substantial alterations (**Figure S1C**). Notably, there was a

224 marked increase in the abundance of iron transport proteins, including SirA, FhuC, SstC, SstD, HtsA,
225 IsdB, IsdE, and IsdI. In addition, elevated levels of ScdA and CntA (Esquilin-Lebron et al., 2021) -
226 proteins involved in iron-sulfur cluster binding - alongside the downregulation of *miaB* (Barrault et
227 al., 2024), suggest the activation of iron-sparing strategies by *S. aureus* under serum conditions
228 (**Tables S2** and **S3**). The significant increase in levels of ScdA and CntA, iron cluster binding proteins
229 concomitant with the downregulation of *miaB*, point to staphylococcal iron-sparing strategies being
230 switched on during serum exposure (**Table S2** and **S3**). Thus, *S. aureus* coordinates enhanced iron
231 uptake with the regulation of iron incorporation into metalloproteins to efficiently manage iron
232 availability during serum exposure (**Figure 2D**, **Figure S1B** and **S3F**).
233
234 Proteins involved in nucleotide metabolism, particularly those associated with the inosine
235 monophosphate (IMP) biosynthetic pathway, were prominently increased across all *S. aureus* isolates
236 (**Figure 2E** and **Figure S3H**). This pathway is central to the synthesis of purine nucleotides such as
237 adenosine monophosphate (AMP) and guanosine monophosphate (GMP), critical molecules for DNA
238 replication, RNA transcription, and cellular proliferation. These shifts underscore the prioritization
239 of iron homeostasis and nucleotide biosynthesis as key adaptive strategies employed by *S. aureus* to
240 support survival and growth in serum.
241

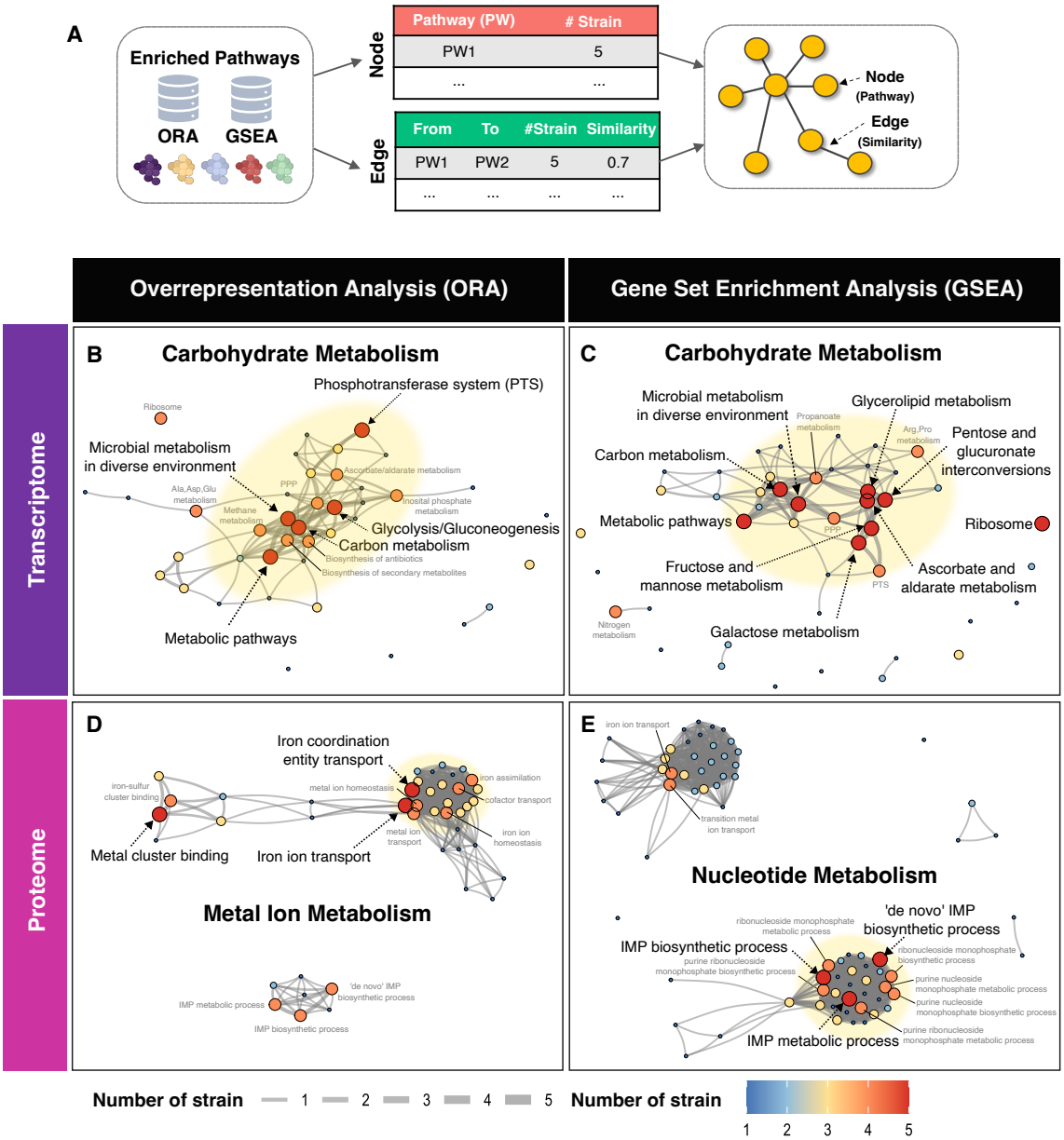

Figure 2. Clustering of transcriptomics and proteomics data into function-related modules

(A) Workflow overview for network analysis of enriched pathways identified from over-representation analysis (ORA) and gene set enrichment analysis (GSEA), with nodes representing pathways and edges representing pairwise similarity (Sim) between enriched terms or pathways (PW), calculated using Jaccard's similarity coefficient. (B-C) ORA and GSEA of transcriptomic data. (D-E) ORA and GSEA of proteomic data. Dot sizes and colors represent the number of strains sharing the same enriched pathways. Edge widths indicate the number of strains with interactions between

251 pathways, while edge lengths reflect pathway similarity. Yellow shading highlights denote
252 functionally related modules.
253

254 **Experimental validation of predicted molecular signatures of *S. aureus* responses to human**
255 **serum**

256 To confirm findings from the multi-omic integration and pathway enrichment analyses, we assessed
257 the fitness of *S. aureus* transposon mutants in genes involved in carbon metabolism, iron acquisition,
258 and oxidative stress resistance, relative to their parental wild-type USA300 JE2 strain, in the presence
259 of serum (**Figures 1E and 3A**). We initially verified the genetic relatedness of the five *S. aureus*
260 bloodstream isolates to the laboratory strain JE2, used for this phenotypic validation. We observed a
261 high conservation of the *S. aureus* core genome (2,222 core genes- representing 71% of JE2 genome-
262 and 903 accessory genes). Strain JE2 was most closely related to the clinical isolate BPH2986, with
263 both belonging to the ST8 USA300 lineage and differing by only 73 single nucleotide polymorphisms
264 (SNPs) (**Figure S4A-D**).

265 The DIABLO integrative model identified *gapdhB* and *sucA* as key contributors to response to
266 serum, exhibiting the highest loading values (**Figure 1D, Table S1)**. Disruption of either gene
267 resulted in a significant reduction in bacterial fitness in serum, highlighting their critical roles in
268 response to serum exposure (**Figure 3B and S5A**).

269 GapdhB, a gluconeogenic enzyme, and SucA, an enzyme of the tricarboxylic acid (TCA) cycle,
270 represent distinct nodes in the carbon metabolism pathway. This functional difference suggests that
271 their contributions to fitness may be contingent upon the availability and type of carbon substrates.
272 To test this, we compared the growth and respiration phenotypes of *gapdhB* and *sucA* mutants using
273 a panel of 190 sole carbon sources (Biolog Inc., Hayward, CA, USA), to that of the wild type S.
274 aureus JE2 strain. These carbon sources fall into several broad categories, including carbohydrates
275 (mono-, di-, and oligosaccharides), carboxylic acids (short-chain fatty acids like acetate, dicarboxylic

276 acids like fumarate, and hydroxy acids like lactate), amino acids, alcohols, nucleosides and other
277 organic compounds that do not fit in the aforementioned classes. The metabolic activities of JE2,
278 *gapdhB* and *sucA* were more strongly influenced by individual carbon sources, irrespective of their
279 broader carbon classification (**Figure S6A**).

280

281 Among the tested substrates, methyl pyruvate, a carboxylic acid and α-D-glucose, D-glucosamine,
282 and other hexoses significantly enhanced respiration in both WT and mutant strains, whereas
283 glyoxylic acid and itaconic acid suppressed respiration (**Figure 3C, Figure S6** and **Table**
284 **S4**). Notably, methyl pyruvate supplementation partially rescued the respiratory deficiency of
285 the *sucA* mutant, surpassing WT levels, while it failed to restore *gapdhB* mutant activity to WT levels
286 (**Figures 3C and S6B**). These findings suggest that while both *gapdhB* and *sucA* are critical for
287 optimal fitness in serum, the encoded enzymes play distinct roles in pyruvate catabolism. Methyl
288 pyruvate, a membrane permeable pyruvate analog, enter cells where it is converted to acetyl-coA. In
289 absence of *sucA,* supplementation with methyl pyruvate provides an alternative carbon source that
290 bypasses the glycolytic block caused by the absence of conversion of 2-oxaloglutarate to succinyl-
291 coA in the TCA cycle. GapdhB catalyzes the conversion of glyceraldehyde-3-phosphate (G3P) to
292 1,3-biphosphoglycerate in the gluconeogenic direction (Purves et al., 2010). In a *gapdhB* mutant, the
293 gluconeogenic pathway is blocked, so cells cannot convert methyl pyruvate (see primary metabolism
294 in **Figure 4**).
295 To investigate the contribution of iron acquisition systems to *Staphylococcus aureus* fitness in serum,
296 we evaluated four transposon mutants (*htsA*, *sirA*, *sstD*, and *isdB*). The *htsA* and *sirA* genes encode
297 substrate-binding proteins associated with the siderophores staphyloferrin A (SA) and staphyloferrin
298 B (SB), respectively, both of which facilitate iron extraction from transferrin in serum (Beasley,
299 Marolda, et al., 2011). The gene *sstD* encodes a component of the Sst system, which mediates iron
300 uptake from host-derived catechols (Beasley, Marolda, et al., 2011). In contrast, *isdB* encodes a cell
301 wall-anchored haemoglobin receptor within the Isd (iron-regulated surface determinant) system, a

302 siderophore-independent pathway that enables heme iron acquisition (**Figure 3D**). Proteomics
303 revealed significantly elevated levels of HtsA, SirA, SstD, and IsdB following serum exposure,
304 indicating their upregulation in response to iron-limited conditions (**Figure S1C**). *S. aureus* mutants
305 with transposon insertions in *sirA* and *sstD* had significantly impaired fitness in serum, consistent
306 with the importance of SB-mediated and catechol-mediated iron uptake under these conditions
307 (**Figure 3E**). In contrast, disruption of *htsA* did not significantly affect fitness, aligned with previous
308 findings that SB biosynthesis, unlike SA, is independent of TCA cycle activity and may be
309 preferentially utilized in iron-restricted environments (Sheldon et al., 2014). The reduced fitness
310 observed in the *sirA* mutant likely reflects the impaired utilization of SB as an iron capture process in
311 serum.

312 Interestingly, the *isdB* mutant exhibited no fitness defect in commercially sourced serum, likely due
313 to the absence of haemoglobin or heme (Pishchany et al., 2014), which are typically sequestered
314 within red blood cells and thus not present in commercial cell-free serum preparations. These findings
315 underscore the context-dependent utilization of iron acquisition systems in *S. aureus* and highlight
316 the critical role of siderophore- and catechol-mediated pathways in supporting staphylococcal
317 survival in iron-limited host environments.
318

319 Oxidative stress constitutes a fundamental component of the host immune response, primarily through
320 the generation of reactive oxygen species (ROS) aimed at neutralizing invading pathogens. To
321 counteract ROS, bacteria have evolved intricate oxidative stress response mechanisms (Imlay, 2008;
322 Toledano et al., 2004). Central to these systems are redox-sensitive transcriptional regulators such as
323 OxyR, PerR, and OhrR, which enable precise detection of specific ROS and orchestrate the
324 staphylococcal defensive gene expression programs (Dubbs & Mongkolsuk, 2012). In *S. aureus*,
325 PerR functions as a principal peroxide sensor and belongs to the ferric uptake regulator (Fur) family
326 of metalloregulatory proteins, which also includes Fur and Zur (Horsburgh et al., 2001). These
327 regulators require metal cofactors for activity, underscoring the metal-dependent nature of oxidative

stress sensing. In our analysis, PerR emerged as a key molecular determinant of oxidative stress resistance in *S. aureus*, a finding that was substantiated through experimental validation (**Figure 3F–G**). The *per* mutant exhibited significant fitness defect in serum supplemented with 0.25- and 0.5 mM hydrogen peroxide (H_2O_2), with the most pronounced impairment observed after 20 hours of exposure to 0.5 mM H_2O_2. These results underscore the critical role of PerR in facilitating *S. aureus* survival under oxidative stress conditions, highlighting its importance in maintaining bacterial fitness in ROS-rich host environments.

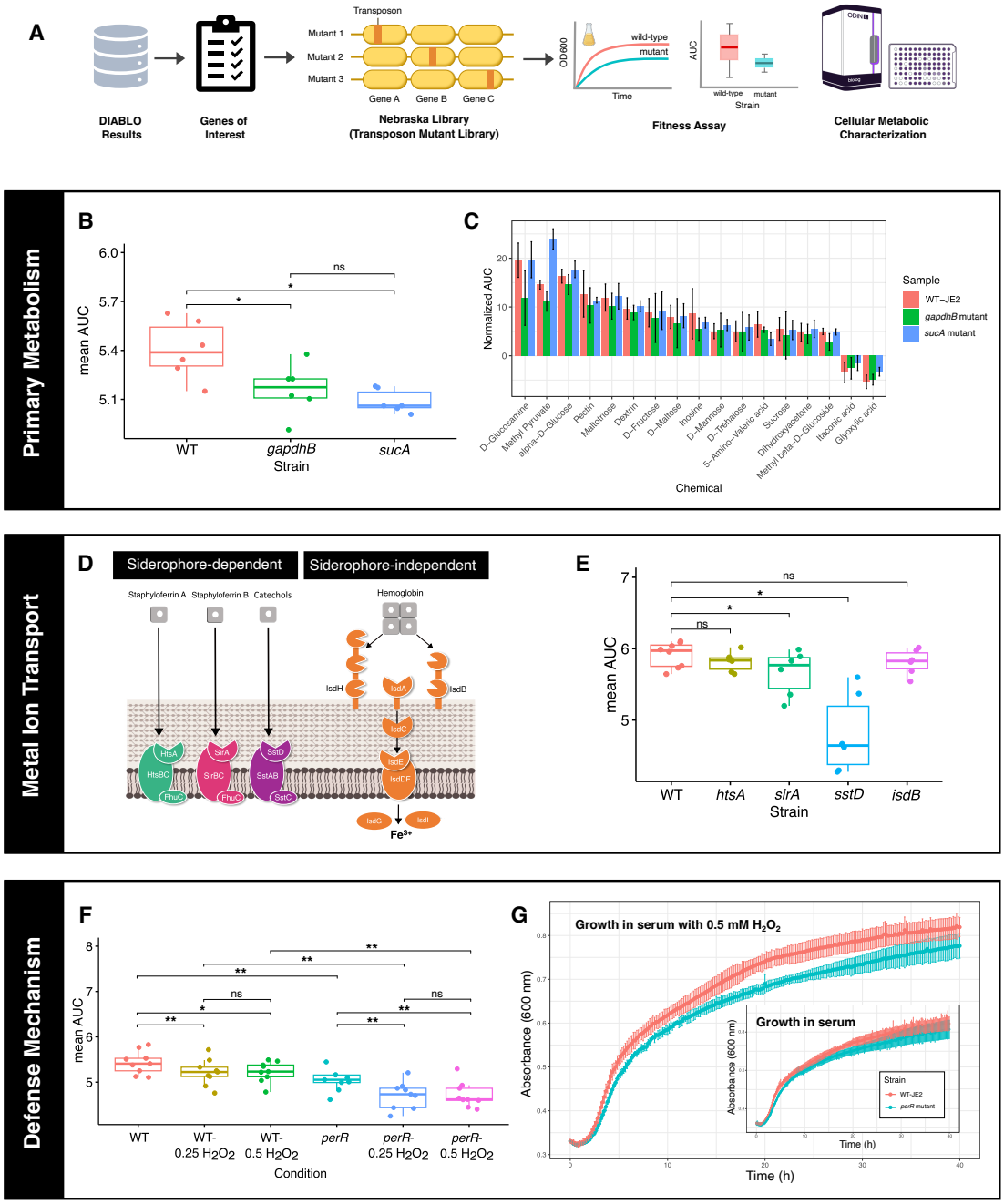

336 **Figure 3. Phenotypic validation of molecular signatures of serum adaptation and metabolic**
337 **characterization**
338 (A) Workflow of phenotypic validation experiments to confirm the predicted molecular signatures of
339 *S. aureus* exposed to human serum. (B) Box plots comparing Area-under-the-curve (AUC) values of
340 *gapdhB* and *sucA* mutants to wild-type *S. aureus* (WT-JE2) grown in presence of serum, for 20 hours.
341 (C) Fitness profiling of *S. aureus* represented by the rate of bacterial respiration in presence of
342 different carbon sources (corresponding to metabolic activity inferred from the reduction of
343 tetrazolium). Plots comparing Area-under-the-curve (AUC) values of *gapdhB* and *sucA* mutants to
344 wild-type *S. aureus* (WT-JE2) grown in presence of sole carbon sources, for 24 hours. (D)
345 Representation of iron acquisition pathways in *S. aureus.* (E) Box plots comparing AUC values of
346 iron transport-deficient mutants (*htsA, sirA, sstD, isdB*) to WT-JE2 cultured in serum for 20 hours.
347 (F) Box plots comparing AUC values of *perR* mutant to WT-JE2 grown in serum with different
348 concentrations of H_2O_2 for 20 hours, demonstrating the role of *perR* in oxidative stress resistance. (G)
349 Representative growth curves for the *S. aureus* WT- JE2 and *perR* mutant grown in serum alone (inset
350 plot) and serum containing H_2O_2 (large plot) over 40 hours. All data points represent mean values for
351 at least three independent biological replicates, with error bars indicating the corresponding standard
352 deviations from the means.
353 Statistical significance between the AUC of WT-JE2 and isogenic mutants was determined using
354 the **Wilcoxon paired test**. Significance levels are indicated by asterisks: *$p < 0.05$, **$p < 0.01$, and
355 ***$p < 0.001$.
356
357 **Integrated metabolic responses of *S. aureus* to human serum**

358 To conceptualize the dynamic remodelling of *S. aureus* metabolism in response to serum, we
359 constructed a scaffolded metabolic network based on curated literature (Beasley, Cheung, et al., 2011;
360 Carvalho et al., 2017; Gaupp et al., 2012; Halsey et al., 2017; Hines et al., 2020; Imada et al., 1977;
361 Kenny et al., 2013; Kriegeskorte et al., 2014; Nolan et al., 2023; O'Connor et al., 2024; Parsons &

362 Rock, 2013; Potter et al., 2020; Qi et al., 2023; Sachla & Helmann, 2019). This network was overlaid
363 with the significant changes in key enzymes identified through single omics (genes upregulated in
364 orange, downregulated in light blue) and by DIABLO integration (genes and metabolites in red),
365 combined with network analyses (**Figure 4, Tables S2–S5**). This integrative approach revealed that
366 *S. aureus* mounts a broad and adaptable metabolic response to the challenges posed by the serum
367 environment, particularly in the utilization of diverse carbon sources including carbohydrates, amino
368 acids, and lipids. Multi-omics data (**Figure S7A–D**) highlighted consistent upregulation of
369 gluconeogenic and TCA cycle enzymes at both transcript and protein levels, indicating a metabolic
370 shift toward energy-efficient carbon utilization upon exposure to serum.
371
372 Carbohydrate metabolism was organized around three key metabolic nodes—glucose-6-
373 phosphate/fructose-6-phosphate (G6P/F6P), glyceraldehyde-3-phosphate/dihydroxyacetone
374 phosphate (GA3P/DHAP), and pyruvate (**Figure 4**, purple nodes embedded in
375 glycolysis/gluconeogenesis)—which serve as convergence points for nutrient assimilation. The
376 upregulation of carbohydrate transporter genes (*uhpT, mtlA, fruA, glcC, lacE, SAUSA300_RS01760,*
377 *rbsU*) in serum aligns with our findings that saccharides, including the hexose monosaccharides α-
378 D-glucose, D-fructose, D-mannose and disaccharides D-maltose, and sucrose, significantly enhanced
379 the metabolic activity of *S. aureus* (**Figures 3C and S6A**). Notably, saccharides such as G6P,
380 fructose, and mannose—but not glucose—have been shown to influence virulence gene expression
381 (Seo et al., 2021). Our transcriptomic data support this, revealing increased expression of γ-
382 hemolysins genes (*hlgA, hlgB, hlgC*) and immune evasion genes (*ecb, sbi, vraX*) across five *S. aureus*
383 strains in serum. In particular, strain BPH2986 (ST8) exhibited strong upregulation of *lukF-*
384 *PV* and *lukS-PV* genes, encoding Panton-Valentine leucocidins (**Figure S8A**). These findings suggest
385 that carbohydrates, such as fructose and mannose, present in serum, support the metabolic activity of
386 *S. aureus* while increasing virulence gene expression, in contrast to the glucose-rich RPMI.
387

388 Amino acids and peptides from serum further contribute to the metabolic adaptability of *S. aureus* by
389 entering carbohydrate metabolism and the TCA cycle through key intermediates such as pyruvate, 2-
390 oxoglutarate, and oxaloacetate. These entry points define three functional groups of amino acids: (1)
391 pyruvate-yielding, (2) 2-oxoglutarate-yielding, and (3) oxaloacetate-yielding (**Figure 4**). Our
392 transcriptomic data revealed significant upregulation of enzymes involved in amino acid catabolism,
393 including *pckA* (encoding pyruvate carboxykinase) and *gudB* (encoding glutamate dehydrogenase),
394 consistent with elevated intracellular levels of phosphoenolpyruvate (PEP) and 2-oxoglutarate
395 (**Figure S7C–E**). Genes encoding enzymes for the degradation of glutamate (*gudB*), proline
396 (*pruA/rocA*, *putA*), arginine (*rocD/argD*), and histidine (*hutI, hutG*) were also upregulated, indicating
397 preferential catabolism of these amino acids during serum exposure. These findings are consistent
398 with previous reports identifying glutamate and its precursors as major carbon sources supporting *S.*
399 *aureus* proliferation (Halsey et al., 2017), positioning glutamate as a central amino acid in the
400 adaptive response to serum.
401
402 Exposure to human serum triggered a marked upregulation of *S. aureus* genes involved in lipid and
403 phospholipid degradation, including *glpQ* and *gehA*. This suggests an enhanced capacity in using
404 host-derived lipids—such as cholesterol, linoleic acid (C18:2), and oleic acid (C18:1)—as nutrient
405 sources. These lipids are metabolized into glycerol-3-phosphate (G3P), which can be then funnelled
406 into the carbohydrate metabolism via the GA3P/DHAP node. Interestingly, our transcriptomic data
407 revealed downregulation of *tpiA*, which encodes triosephosphate isomerase, an enzyme responsible
408 for the reversible interconversion of GA3P and DHAP. This suggests a potential bottleneck at this
409 metabolic junction, which may constrain glycolytic flux and influence the efficiency of carbon
410 utilization from lipids present in serum.
411
412 Counteracting innate immune defences is essential for *S. aureus* survival during bloodstream
413 infection. Upon exposure to human serum, *S. aureus* exhibited robust transcriptional upregulation of

414 a broad range of virulence-associated genes involved in immune evasion, host colonization, and
415 pathogenesis. These include genes encoding complement-evasion proteins (*ecb, sbi, vraX*), pore-
416 forming cytotoxins (*hlgA, hlgB, hlgC*), superantigen-like proteins (*ssl13, ssl14*), and the fibrinogen-
417 binding adhesin *clfA*. This coordinated immune evasion strategy underscores the pathogen's capacity
418 to rapidly adapt to immune pressures and enhance its invasive potential in the bloodstream.
419
420 Serum exposure also elicited a pronounced oxidative stress response in *S. aureus*. DIABLO analysis
421 identified *perR,* which encodes the peroxide-sensing transcriptional regulator PerR, as a key
422 molecular signature of staphylococcal adaptation to serum. Consistent with this, genes involved in
423 carotenoid biosynthesis —*crtM, crtN, crtQ* —were upregulated, suggesting enhanced anti-oxidative
424 defence through increased production of staphyloxanthin, a carotenoid pigment known to protect
425 against reactive oxygen species (Clauditz et al., 2006). In parallel, elevated expression of *scdA*, a gene
426 involved in iron-sulphur cluster repair, indicates activation of protein maintenance pathways essential
427 for preserving enzymatic and cellular functions under oxidative stress (Chang et al., 2006; Overton
428 et al., 2008).
429
430 Collectively, our integrative approach highlighted the strong adaptive capacity of *S. aureus* to
431 withstand the survival challenges imposed by human serum. Through the coordinated activation of
432 nutrient acquisition systems, oxidative stress defences, and virulence-associated mechanisms, *S.*
433 *aureus* enhances its ability to survive and persist during systemic infection.
434

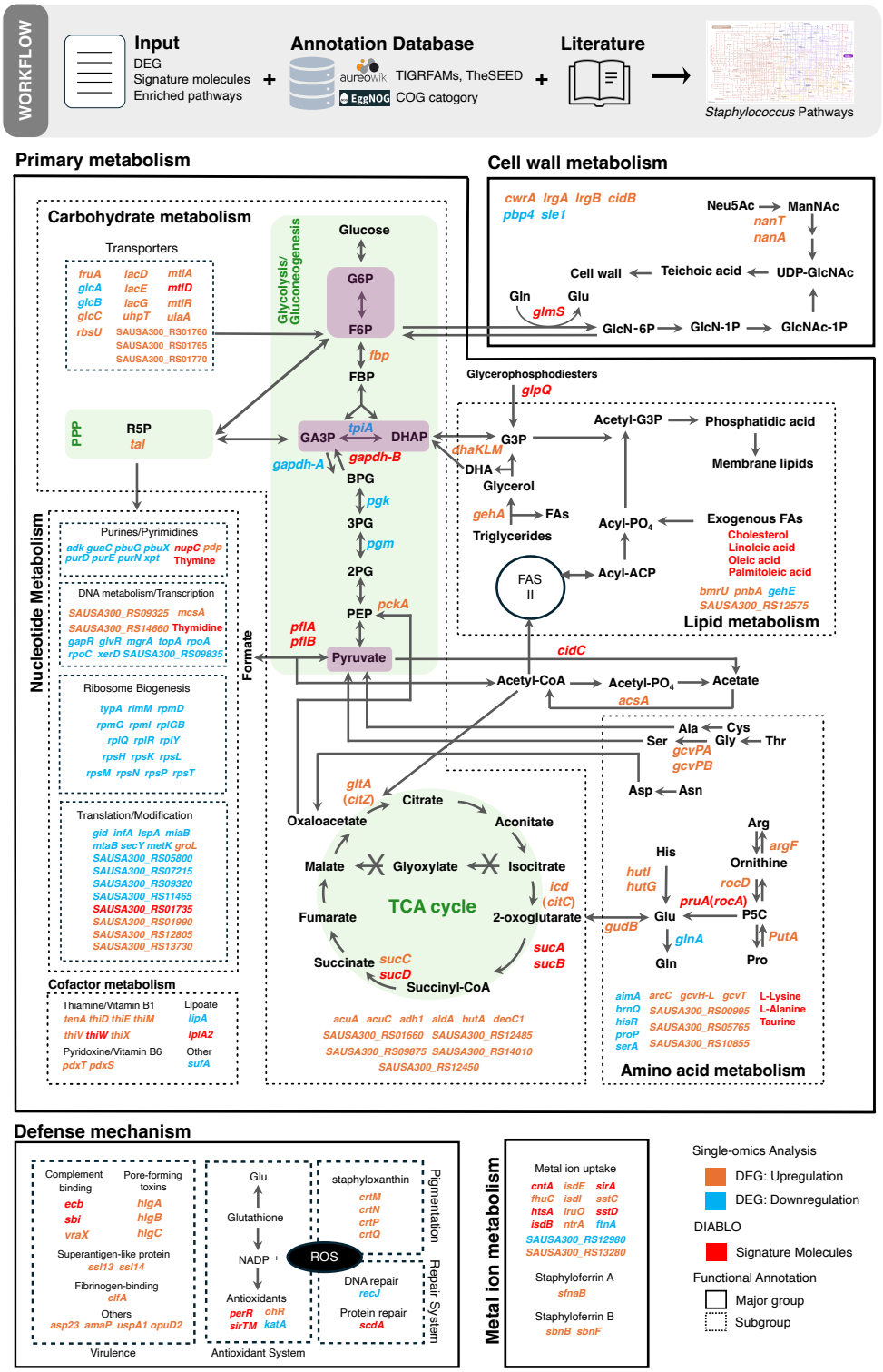

Figure 4. Integrated metabolic and virulence adaptation of *S. aureus* in response to serum

Systems-level metabolic reprogramming of *S. aureus* upon exposure to serum, integrating single- and multi-omics data. The depicted key metabolic pathways include glycolysis/gluconeogenesis (upright rectangle shaded in light green), the pentose phosphate pathway (PPP), the tricarboxylic acid (TCA) cycle (circle shaded in light green), nucleotide biosynthesis, ribosome biogenesis, thiamine (vitamin

441 B1) biosynthesis and transport, cell wall biosynthesis, and lipid metabolism. Host-responsive
442 processes such as immune evasion, metal ion acquisition, and oxidative stress responses are also
443 represented. The name of enzyme is colored to indicate changes in gene expression following serum
444 exposure identified by single omics (compared to RPMI), with orange: increased expression, light
445 blue: decreased expression. Variables predicted by DIABLO (multi-omics analysis) are in red,
446 indicating their status as signature molecules of *S. aureus* serum response.

447

448 **Discussion**

449 Whilst a leading cause of lethal bacteraemia, *S. aureus* must contend with the nutrient-limited and
450 immunologically hostile conditions of the bloodstream to establish infection and cause disease. In the
451 bloodstream, the bacterium uses a large panoply of virulence factors to evade clearance by cellular
452 and humoral immunity (Cheung et al., 2021; Howden et al., 2023; Soe et al., 2021). Notwithstanding
453 the bactericidal activities of immune cells patrolling the bloodstream, serum remains a challenging
454 environment for *S. aureus* due to the paucity of free forms of essential nutrients, often complexed to
455 large proteins (e.g. iron ions complexed to transferrin) (Ledala et al., 2014). Several studies have
456 shown that *S. aureus* has evolved multiple mechanisms, not related to its cytotoxicity, to overcome
457 the nutritional constrains and acellular insults of the serum (Murdoch &Skaar, 2022). While
458 informing on discrete *S. aureus* coping mechanisms to survive nutritional stress, these studies focused
459 on staphylococcal genes and pathways in isolation and did not consider the concomitant adaptive
460 responses to the serum environment. Building on our previous work showing that four
461 phylogenetically diverse blood invasive pathogens, including *S. aureus*, adapted to serum by
462 remodelling their cell wall envelopes (Mu et al., 2023), we employed a multi-omics framework to
463 determine the commonly shared *S. aureus* adaptive response to serum across five distinct clinical
464 isolates. Such approach offers a systems-level view of microbial adaptation in response to
465 environmental stimuli, by linking molecular changes across genomic, transcriptomic, proteomic, and
466 metabolomic layers (Fouché & Zinovyev, 2023; Maghsoudi et al., 2022; Vahabi & Michailidis,

467 2022). Using integrative machine learning-based multivariate analyses, differential expression
468 profiling, and network-based approaches, our study identified staphylococcal reprogramming in cell
469 wall biosynthesis, carbon metabolism, iron transport, and defence mechanisms in response to serum.
470
471 The experimental validation of the dominant outputs identified by our integrative framework
472 confirmed the importance of *gapdhB*, *sucA*, *sirA*, *sstD*, and *perR* genes for staphylococcal fitness in
473 serum (**Figure 3**). These results align with the positive co-variation patterns observed in the DIABLO
474 model, suggesting a functional interdependence among the pathways involving these genes (**Figure**
475 **1C**). Whilst critical for optimal fitness in serum, *gapdhB* and *sucA* have distinct functions in carbon
476 metabolism. Metabolic profiling revealed that hexose saccharides (e.g., α-D-glucose, D-glucosamine)
477 enhanced the metabolic activity in WT and *gapdhB* and *sucA* mutants, through glycolysis,
478 gluconeogenesis, PPP, and TCA cycle. While methyl pyruvate partially restored bacterial respiration
479 in the *sucA* mutant, likely via conversion to acetyl-CoA and oxaloacetate (Campbell et al., 2021), the
480 *gapdhB* mutant remained metabolically impaired, reflecting incomplete gluconeogenesis and
481 insufficient PPP intermediate generation (**Figures 3B** and **S6**). While highlighting the importance of
482 gluconeogenesis for *S. aureus* during serum exposure, these results further underscore the non-
483 redundant roles of GAPDH homologs (*gapdhA*, *gapdhB*) in maintaining metabolic flux (Purves et al.,
484 2010). Interestingly, pyruvate was shown to activate *S. aureus* regulatory networks controlling the
485 production of leucocidins, and thus, potentiating the cytotoxicity of *S. aureus* (Harper et al., 2018).
486 Conversely, exposure to glyoxylate and itaconate inhibited *S. aureus* metabolism **(Figures 3C** and
487 **S6)**. The bacterium lacks a glyoxylate shunt, rendering glyoxylate toxic due to metabolic imbalance.
488 Moreover, glyoxylate is limited in serum, as humans lack an active glyoxylate cycle (Halsey et al.,
489 2017). Itaconate, an immunometabolite produced by macrophages, further exacerbates stress by
490 directly inhibiting glycolysis (Tomlinson et al., 2021; Tomlinson & Riquelme, 2021). These findings
491 highlight the potential of *S. aureus* metabolic vulnerabilities that could be exploited therapeutically.
492 We constructed a metabolic scaffold of *S. aureus* that integrates the predicted signature molecules

493 elicited/repressed in serum (**Figure 4, Table S4**). This illustrates the impressive flexibility of the
494 pathogen in using diverse carbon sources in serum, such as hexose saccharides, amino acids yielding
495 2-oxoglutarate (e.g., Glu, Pro, Arg, His), and host lipids and fatty acids (e.g., cholesterol, linoleic acid
496 (C18:2), and oleic acid (C18:1)) to support its fitness and virulence. Hexose saccharides have been
497 shown to regulate virulence gene expression (Seo et al., 2021). Peptides and amino acids present in
498 serum contribute to *S. aureus* metabolism by entering the glycolysis via pyruvate or intermediates of
499 the TCA cycle (e.g., 2-oxoglutarate, oxaloacetate). Transcriptomic analysis revealed significant
500 upregulation of key enzymes involved in amino acid catabolism, including pyruvate carboxykinase
501 (*pckA*) and glutamate dehydrogenase (*gudB*), phosphoenolpyruvate (PEP) and 2-oxoglutarate
502 (**Figure S7C-E**). Notably, we found a significant increase in gene expression of enzymes (e.g. *gudB*,
503 *pruA*(*rocA*), *putA, rocD(argD), hutI,* and *hutG*) converting amino acids (e.g., Glu, Pro, Arg, His) to
504 2-oxoglutarate in amino acid catabolism, indicating the usage of these amino acids in serum. This is
505 consistent with the observation that glutamate, and the amino acids that can be converted into
506 glutamate (Pro, Arg, and His), provide most of the carbon required for cell proliferation (Halsey et
507 al., 2017). Several upregulated metabolic pathways facilitating glutamate production, driven by *pruA*
508 (converting proline to glutamate) and *putA* (proline dehydrogenase) underline glutamate as a key
509 intermediate metabolite in the adaptive response to serum. Concurrently, the downregulation of
510 glutamine synthesis, through decreased expression of GlnA, suggests a reduction in the utilization of
511 glutamate. Although excess levels of glutamate did not significantly influence the respiration or
512 fitness of WT-JE2 (**Table S4**), several studies have highlighted the important role of glutamate in
513 protecting bacteria from cell death under stress (Ramond et al., 2014; Tavares et al., 2011; Yee et al.,
514 2015; Yee et al., 2019).
515
516 Iron is an important determinant for *S. aureus* fitness and virulence (Ledala et al., 2014). Our analyses
517 further confirm the engagement of multiple iron acquisition mechanisms to cope with iron-limited
518 host environments such as the serum. Interestingly, mutants lacking *htsA* and *isdB*, both involved in

519 iron acquisition, displayed fitness levels comparable to that of the wild-type (WT-JE2), suggesting
520 their potential redundancy within the iron uptake systems and adaptation to the serum's low free iron
521 levels (**Figure 3E**). This is consistent with prior findings reporting the upregulation of iron acquisition
522 systems such as Isd and SirABC in *S. aureus* cultured in serum or blood (Malachowa et al., 2011).
523 Further studies are necessary to understand the specificity of iron-acquisition modules in iron-limited
524 environments in the context of bacterial metabolic reprograming during bloodstream infection.
525
526 Serum exposure also elicited the engagement of *S. aureus* defence mechanisms against acellular
527 immunity. Our analytical framework highlighted the upregulation of virulence-related genes (**Figures**
528 **4 and S8)**. These include complement-binding proteins (e.g., *ecb*, *sbi*, *vraX*) (Haupt et al., 2008;
529 Jongerius et al., 2010; Yan et al., 2017), pore-forming toxins (e.g., the γ-haemolysins *hlgA*, *hlgB*,
530 *hlgC*) (Spaan et al., 2014), superantigen-like proteins (*ssl13*, *ssl14*) (Zhao et al., 2018), and the
531 fibrinogen-binding protein *clfA* (Higgins et al., 2006). Such responses would prime *S. aureus* against
532 clearance by immune cells. The identification of immunoglobulin-binding protein (Sbi) and
533 complement convertase inhibitor (Ecb), both enabling evasion from host antibodies and the
534 complement system (Jongerius et al., 2010; Smith et al., 2011) as signatures by DIABLO reinforce
535 the pertinence of using multi-omics analysis for the identification of bacterial responses relevant to
536 environmental conditions. The *S. aureus* sensing and response to host oxidative stress were also
537 highlighted as essential for optimal fitness in serum (Horsburgh et al., 2001; Ji et al., 2015; Rack et
538 al., 2015; Rack et al., 2020).
539
540
541 **Conclusion and perspectives**

542 This study exploited multi-omics analyses, including machine learning-based approaches, DE
543 analysis and network analysis, to uncover key *S. aureus* signature molecules responding to human
544 serum. Our findings highlight the concomitant activation of nutrient acquisition systems, oxidative

545 stress defences, and virulence-associated mechanisms, underlining the strong adaptive capacity of *S.*
546 *aureus* to withstand the multifactorial challenges imposed by human serum. While serum is acellular
547 and does not reflect the breadth of host-pathogen interactions during bloodstream infections, this
548 matrix is a useful proxy for understanding how invading bacteria survive in blood. Our multi-omic
549 analytical approach identified key staphylococcal pathways that could be further studied to continue
550 dissecting staphylococcal adaptive responses and to identify bacterial (and host) targets for new
551 therapeutic approaches.
552
553 **Limitations of the study**
554 The integrative analysis performed here was highly sensitive and detected subtle patterns linking
555 different omic datasets. However, the metabolic flexibility and functional redundancy within key
556 bacterial pathways - particularly central carbon metabolism and iron acquisition – are likely not
557 limited to individual contributions of specific genes, thus making genes contributing to these
558 pathways difficult to confirm experimentally using single isogenic mutants. Furthermore, the
559 individual contributions of metabolites such as citrate, an intermediate of the TCA cycle, can repress
560 the activity of the transcriptional activity of genes involved in iron homeostasis (Chen et al., 2024),
561 underscoring the cross-talks between pathways that could alter single -omic readouts, and thus multi-
562 omics analyses. This study used commercially sourced serum for phenotypic confirmation of the
563 staphylococcal signatures. Whilst such reagent offers more control, such as batch control, the
564 concentrations of carbohydrates, metal ions, and reactive oxygen species are unknown, which may
565 influence the significance of phenotypic outputs.
566
567
568
569
570

571 **METHODS**

572

573 ***S. aureus* genome and pangenome analyses**

574 The complete genomes of five clinical *S. aureus* strains, BPH2760, BPH2819, BPH2900, BPH2947,
575 BPH2986 (Mu et al., 2023), and of the strain USA300 JE2 were downloaded from the NCBI database
576 (https://www.ncbi.nlm.nih.gov/bioproject/PRJEB29881/, https://www.ncbi.nlm.nih.
577 gov/bioproject/PRJNA381486).

578 Genomic analysis was conducted using Bohra v2.3.6 (https://github.com/MDU-PHL/bohra). Bohra
579 provided information such as Single Nucleotide Polymorphisms (SNPs), phylogeny, multi-locus
580 sequence typing (MLST), resistome, virulome, and Pan-genome. We used Phandango to visualize the
581 pangenome profiles (https://jameshadfield.github.io/phandango/#/).

582 The AureoWiki database (Fuchs et al., 2018) was used to annotate *S. aureus* genes/proteins and to
583 define orthologous relationships, through a reciprocal best hit (RBH) search using MMseqs2 with
584 default parameters (https://github.com/soedinglab/MMseqs2) between the five studied genomes
585 (FAA format) and the *S. aureus* reference genome and proteome (USA300_FPR3757_NCBI_2017
586 and USA300_FPR3757_NCBI_UniProt_2013).

587

588 **Confirmation of *S. aureus* transposon mutants' genome sequence**

589 We used *S. aureus* transposon mutants of signature genes identified by our analytical pipeline, to
590 verify their fitness in serum. These mutants were selected from the Nebraska transposon library
591 (NTL), including NE275, NE400, NE547, NE665, NE1102, NE1343, and NE1767 (Fey et al., 2013).
592 The mutants are expected to contain a precise and non-polar transposon insertions, without additional
593 mutations. All mutants were genome sequenced on the Oxford Nanopore platform using Min114 flow
594 cells. Base calling, demultiplexing, and adapter removal were performed in real-time using
595 MinKNOW. Mutant NE1102 was sequenced on a GridION and processed using Guppy. Remaining
596 mutants were sequenced on a MinION and processed using Dorado. FASTQ reads were assembled

597 using Trycycler version 0.5.3 (Wick et al., 2021). The assembled genomes were compared to the
598 cognate wild-type reference genome using the Mauve whole-genome aligner plugin tool in the
599 Geneious Prime (version 2022.2.2) (https://www.ncbi.nlm.nih.gov/pmc/ articles/PMC442156/).
600
601 ***S. aureus* fitness in serum**
602 We used batch-controlled human serum (Male AB plasma, Sigma Aldrich) to reduce variations
603 arising from different donors. Human serum was clarified from lipids by centrifugation at 3,000 x g
604 during 5 min at 4°C. Overnight cultures of *S. aureus* JE2 (WT), and NTL mutants of *gapdhB*, *sucA*,
605 *htsA*, *sirA*, *sstD*, *isdB* and *perR* were grown from single colonies in 10 ml Brain Heart Infusion media
606 (BHI, BD BACTO™) at 37 °C with orbital shaking. Overnight cultures were centrifuged for 5 min
607 at 5,000 x g, and pellets were washed twice with sterile PBS. The cells were then standardized to an
608 OD 600 nm = 0.5 (0.5 UOD) in RPMI (Gibco™). Bacteria equivalent to 0.01 UOD were inoculated
609 in 180 µL of BHI, RPMI or 50% serum (diluted in RPMI) in clear 96-well plate (Costar), in triplicate
610 to a final volume of 200 µL. Plates were incubated at 37°C in ClariostarPLUS microplate reader
611 (BMG Labtech) and bacterial growth was measured every 10 min for 20 h at 600 nm.
612
613 **Phenotypic analysis of *S. aureus* carbohydrate metabolism**
614 Phenotypic profiling was performed using the Biolog Phenotype MicroArray™ (PM) system with
615 PM1 and PM2 plates (Biolog Inc., Hayward, CA, USA), to determine the *S. aureus* fitness in presence
616 of 190 distinct carbon sources. Overnight *S. aureus* cultures were grown in BHI at 37 °C with
617 shaking. Bacterial suspensions were prepared according to the manufacturer's protocol for Gram-
618 positive organisms. The inocula of *gapdhB*, *sucA* and parental WT strain were loaded into PM1 and
619 PM2 plates and incubated at 37 °C for 24 hours in the Biolog Odin™ system, which enables the
620 simultaneous monitoring of growth and respiration (by redox dye reduction). Metabolic activity was
621 assessed by measuring the reduction of tetrazolium-based redox dyes, which serve as indicators of
622 electron transport chain activity in response to specific carbon sources. Dye reduction results in the

623 formation of purple formazan, with absorbance recorded every 20 minutes at 590 nm. The area under
624 the curve (AUC) for each well was calculated to quantify metabolic activity, enabling comparative
625 analysis of carbon source utilization across conditions or strains.
626
627 **Principal component analysis**
628 Principal Component Analysis (PCA) was independently performed on each omics dataset—
629 transcriptomics, proteomics, GC-MS metabolomics, and LC-MS metabolomics—to explore global
630 data structure and identify the primary sources of variation between serum- and RPMI-exposed
631 samples. PCA was conducted using the *pca()* function from the mixOmics package (v6.24.0) in R
632 (v4.2.3), with data scaled to unit variance. The optimal number of components was determined using
633 the tune.pca() function, which indicated that the first three components captured approximately 50%
634 of the total variance across datasets.
635
636 **Multi-omics data integration**
637 We implemented the MixOmics data analytic pipeline known as Multiblock (s)PLS-DA or DIABLO,
638 a multivariate statistical method for classifying and separating different categorical classes (Rohart et
639 al., 2017; Singh et al., 2019). This supervised multi-omics integrative method adds sparsity to the
640 model, improving result interpretability by selecting the most relevant variables and setting others'
641 coefficients to zero. DIABLO treats each omics dataset as a separate "block" and identifies co-
642 variation patterns across these blocks, to determine interactions between, and changes by, biological
643 molecules under various conditions. The DIABLO model was designed with a selected design matrix
644 weight of 0.5 to balance discrimination between conditions and correlation across omics layers,
645 ensuring that feature selection prioritised both inter-omics agreement and RPMI-Serum separation.
646 An initial model trained with five components revealed that the first component alone was sufficient
647 to clearly discriminate between serum and RPMI conditions. To assess model robustness and guide
648 component selection, we performed leave-one-out (LOO) cross-validation, which confirmed that a

649 single component provided perfect classification performance. To optimize feature selection for each
650 omics layer, we performed parameter tuning using the tune.block.splsda function. A grid of candidate
651 values for the number of features to retain per block was defined: 20–100 (step size 20) for
652 transcriptomics and proteomics, and 10–100 (step size 10) for both metabolomics datasets (GC-MS
653 and LC-MS). The model was tuned using 5-fold cross-validation repeated 10 times and centroid
654 distance as the classification metric. The number of features retained per block was: 20 for
655 transcriptomics, 20 for proteomics, 10 for GC-MS, and 10 for LC-MS, totalling 60 features. Using
656 these parameters, the final DIABLO model was built using block.splsda function with one component
657 (as determined during component tuning).(Rohart et al., 2017; Singh et al., 2019)
658

659 **Enrichment analysis**

660 To identify staphylococcal pathways prominently represented following exposure to serum, feature
661 lists derived from all omics data underwent pathway enrichment analysis, using over-representation
662 analysis (ORA) and Gene Set Enrichment Analysis (GSEA). Pathway enrichment analysis was
663 performed with package clusterProfiler v4.6.2. The obtained feature lists were mapped to the
664 associated biological annotation terms (e.g. GO terms or KEGG pathways) and statistical tests for
665 enrichment probability (enrichment P-value) were calculated to obtain the enrichment of the feature
666 sets. In ORA, the preselected features were filtered by a criterion of log2FC > 1 and p-value < 0.05.
667 For GSEA, all features were ranked based on their log2FC values, meaning features with the largest
668 positive and negative expression changes are positioned at opposite ends of the ranked list, while
669 those with smaller or no changes are located near the middle.
670

671 **Network analysis**

672 The biological relationships among the list of enriched pathways were identified by selecting the
673 significant pathways with p.adjust < 0.05 (except for metabolomic datasets; p-value < 0.05). Further
674 network analysis, using pairewise_termsim function in the enrichplot package in R, calculated the

675 pairwise similarity of the enriched terms using Jaccard's similarity coefficient or the similarity of
676 gene subsets sharing between pathways. Conversion to enrichment map to dataframes provided
677 similarity scores and number of strains sharing individual enriched pathways, represented as node
678 and edge, respectively, for networks' visualization.
679

680 **Data availability**

681 All codes are available on GitHub (https://github.com/warasinee/Multiomics_Analyses_2024).
682 Oxford Nanopore reads of all strains and mutants generated are deposited in NCBI SRA (BioProject
683 ID PRJNA1284587).
684

685 **Acknowledgements**

686 This research was supported by the Development and Promotion of Science and Technology Talents
687 Project (DPST) from the Thai Government (WM), the National Health and Medical Research Council
688 of Australia to BPH (GNT1196103), TPS (GNT1194325), AH, SGG, RG (GNT2018880).
689

690 **References**

691 Alfeo, M. J., Pagotto, A., Barbieri, G., Foster, T. J., Vanhoorelbeke, K., De Filippis, V., Speziale,
692 P., & Pietrocola, G. (2021). Staphylococcus aureus iron-regulated surface determinant
693 B (IsdB) protein interacts with von Willebrand factor and promotes adherence to
694 endothelial cells. *Sci Rep*, *11*(1), 22799. https://doi.org/10.1038/s41598-021-02065-w
695 Arragain, S., Handelman, S. K., Forouhar, F., Wei, F. Y., Tomizawa, K., Hunt, J. F., Douki, T.,
696 Fontecave, M., Mulliez, E., & Atta, M. (2010). Identification of eukaryotic and
697 prokaryotic methylthiotransferase for biosynthesis of 2-methylthio-N6-
698 threonylcarbamoyladenosine in tRNA. *J Biol Chem*, *285*(37), 28425-28433.
699 https://doi.org/10.1074/jbc.M110.106831
700 Barrault, M., Leclair, E., Kumeko, E. K., Jacquet, E., & Bouloc, P. (2024). Staphylococcal sRNA
701 IsrR downregulates methylthiotransferase MiaB under iron-deficient conditions.
702 *Microbiol Spectr*, *12*(10), e0388823. https://doi.org/10.1128/spectrum.03888-23
703 Bear, A., Locke, T., Rowland-Jones, S., Pecetta, S., Bagnoli, F., & Darton, T. C. (2023). The
704 immune evasion roles of Staphylococcus aureus protein A and impact on vaccine
705 development. *Front Cell Infect Microbiol*, *13*, 1242702.
706 https://doi.org/10.3389/fcimb.2023.1242702
707 Beasley, F. C., Cheung, J., & Heinrichs, D. E. (2011). Mutation of L-2,3-diaminopropionic acid
708 synthase genes blocks staphyloferrin B synthesis in Staphylococcus aureus. *BMC*
709 *Microbiol*, *11*, 199. https://doi.org/10.1186/1471-2180-11-199

Beasley, F. C., Marolda, C. L., Cheung, J., Buac, S., & Heinrichs, D. E. (2011). Staphylococcus aureus transporters Hts, Sir, and Sst capture iron liberated from human transferrin by Staphyloferrin A, Staphyloferrin B, and catecholamine stress hormones, respectively, and contribute to virulence. *Infect Immun*, *79*(6), 2345-2355. https://doi.org/10.1128/iai.00117-11

Bertrand, B. P., Heim, C. E., West, S. C., Chaudhari, S. S., Ali, H., Thomas, V. C., & Kielian, T. (2022). Role of Staphylococcus aureus Formate Metabolism during Prosthetic Joint Infection. *Infect Immun*, *90*(11), e0042822. https://doi.org/10.1128/iai.00428-22

Brunskill, E. W., de Jonge, B. L. M., & Bayles, K. W. (1997). The Staphylococcus aureus scdA gene: a novel locus that affects cell division and morphogenesis. *Microbiology (Reading)*, *143 (Pt 9)*, 2877-2882. https://doi.org/10.1099/00221287-143-9-2877

Burman, J. D., Leung, E., Atkins, K. L., O'Seaghdha, M. N., Lango, L., Bernadó, P., Bagby, S., Svergun, D. I., Foster, T. J., Isenman, D. E., & van den Elsen, J. M. (2008). Interaction of human complement with Sbi, a staphylococcal immunoglobulin-binding protein: indications of a novel mechanism of complement evasion by Staphylococcus aureus. *J Biol Chem*, *283*(25), 17579-17593. https://doi.org/10.1074/jbc.M800265200

Campbell, C., Fingleton, C., Zeden, M. S., Bueno, E., Gallagher, L. A., Shinde, D., Ahn, J., Olson, H. M., Fillmore, T. L., Adkins, J. N., Razvi, F., Bayles, K. W., Fey, P. D., Thomas, V. C., Cava, F., Clair, G. C., & O'Gara, J. P. (2021). Accumulation of Succinyl Coenzyme A Perturbs the Methicillin-Resistant Staphylococcus aureus (MRSA) Succinylome and Is Associated with Increased Susceptibility to Beta-Lactam Antibiotics. *mBio*, *12*(3), e0053021. https://doi.org/10.1128/mBio.00530-21

Carvalho, S. M., de Jong, A., Kloosterman, T. G., Kuipers, O. P., & Saraiva, L. M. (2017). The Staphylococcus aureus α-Acetolactate Synthase ALS Confers Resistance to Nitrosative Stress. *Front Microbiol*, *8*, 1273. https://doi.org/10.3389/fmicb.2017.01273

Cassat, J. E., & Skaar, E. P. (2012). Metal ion acquisition in Staphylococcus aureus: overcoming nutritional immunity. *Semin Immunopathol*, *34*(2), 215-235. https://doi.org/10.1007/s00281-011-0294-4

Chang, W., Small, D. A., Toghrol, F., & Bentley, W. E. (2006). Global transcriptome analysis of Staphylococcus aureus response to hydrogen peroxide. *J Bacteriol*, *188*(4), 1648-1659. https://doi.org/10.1128/jb.188.4.1648-1659.2006

Chen, F., Zao, Q., Yang, Z., Chen, R., Pan, H., Wang, Y., Liu., H., Cao, Q., Gan, J., Liu, X, Zhang, N., Liang., H &Lan, L. (2024) PLoS Pathogen, e1012425. https://doi.org/10.1371/journal.ppat.1012425

Cheung, G. Y. C., Bae, J. S., & Otto, M. (2021). Pathogenicity and virulence of Staphylococcus aureus. *Virulence*, *12*(1), 547-569. https://doi.org/10.1080/21505594.2021.1878688

Christgen, S. L., & Becker, D. F. (2019). Role of Proline in Pathogen and Host Interactions. *Antioxid Redox Signal*, *30*(4), 683-709. https://doi.org/10.1089/ars.2017.7335

Clauditz, A., Resch, A., Wieland, K. P., Peschel, A., & Götz, F. (2006). Staphyloxanthin plays a role in the fitness of Staphylococcus aureus and its ability to cope with oxidative stress. *Infect Immun*, *74*(8), 4950-4953. https://doi.org/10.1128/iai.00204-06

Cox, M., & Nelson, D. (2008). *Lehninger Principles of Biochemistry* (5 ed.). W. H. Freeman and Company.

de Jong, N. W. M., van Kessel, K. P. M., & van Strijp, J. A. G. (2019). Immune Evasion by Staphylococcus aureus. *Microbiol Spectr*, *7*(2). https://doi.org/10.1128/microbiolspec.GPP3-0061-2019

Dubbs, J. M., & Mongkolsuk, S. (2012). Peroxide-sensing transcriptional regulators in bacteria. *J Bacteriol*, *194*(20), 5495-5503. https://doi.org/10.1128/jb.00304-12

758 Esquilin-Lebron, K., Dubrac, S., Barras, F., & Boyd, J. M. (2021). Bacterial Approaches for
759 Assembling Iron-Sulfur Proteins. *mBio*, *12*(6), e0242521.
760 https://doi.org/10.1128/mBio.02425-21
761 Fey, P. D., Endres, J. L., Yajjala, V. K., Widhelm, T. J., Boissy, R. J., Bose, J. L., & Bayles, K. W.
762 (2013). A genetic resource for rapid and comprehensive phenotype screening of
763 nonessential Staphylococcus aureus genes. *mBio*, *4*(1), e00537-00512.
764 https://doi.org/10.1128/mBio.00537-12
765 Fuchs, S., Mehlan, H., Bernhardt, J., Hennig, A., Michalik, S., Surmann, K., Pané-Farré, J.,
766 Giese, A., Weiss, S., Backert, L., Herbig, A., Nieselt, K., Hecker, M., Völker, U., &
767 Mäder, U. (2018). AureoWiki -The repository of the Staphylococcus aureus research
768 and annotation community. *Int J Med Microbiol*, *308*(6), 558-568.
769 https://doi.org/10.1016/j.ijmm.2017.11.011
770 Gaupp, R., Ledala, N., & Somerville, G. A. (2012). Staphylococcal response to oxidative
771 stress. *Front Cell Infect Microbiol*, *2*, 33. https://doi.org/10.3389/fcimb.2012.00033
772 Ghssein, G., Brutesco, C., Ouerdane, L., Fojcik, C., Izaute, A., Wang, S., Hajjar, C., Lobinski,
773 R., Lemaire, D., Richaud, P., Voulhoux, R., Espaillat, A., Cava, F., Pignol, D., Borezée-
774 Durant, E., & Arnoux, P. (2016). Biosynthesis of a broad-spectrum nicotianamine-like
775 metallophore in Staphylococcus aureus. *Science*, *352*(6289), 1105-1109.
776 https://doi.org/10.1126/science.aaf1018
777 Gibbs, M. R., Moon, K. M., Warner, B. R., Chen, M., Bundschuh, R., Foster, L. J., & Fredrick, K.
778 (2020). Functional Analysis of BipA in E. coli Reveals the Natural Plasticity of 50S
779 Subunit Assembly. *J Mol Biol*, *432*(19), 5259-5272.
780 https://doi.org/10.1016/j.jmb.2020.07.013
781 Grim, K. P., San Francisco, B., Radin, J. N., Brazel, E. B., Kelliher, J. L., Párraga Solórzano, P.
782 K., Kim, P. C., McDevitt, C. A., & Kehl-Fie, T. E. (2017). The Metallophore Staphylopine
783 Enables Staphylococcus aureus To Compete with the Host for Zinc and Overcome
784 Nutritional Immunity. *mBio*, *8*(5). https://doi.org/10.1128/mBio.01281-17
785 Guerra, F. E., Borgogna, T. R., Patel, D. M., Sward, E. W., & Voyich, J. M. (2017). Epic Immune
786 Battles of History: Neutrophils vs. Staphylococcus aureus. *Front Cell Infect Microbiol*,
787 *7*, 286. https://doi.org/10.3389/fcimb.2017.00286
788 Gustafson, J., Strässle, A., Hächler, H., Kayser, F. H., & Berger-Bächi, B. (1994). The femC
789 locus of Staphylococcus aureus required for methicillin resistance includes the
790 glutamine synthetase operon. *J Bacteriol*, *176*(5), 1460-1467.
791 https://doi.org/10.1128/jb.176.5.1460-1467.1994
792 Halsey, C. R., Lei, S., Wax, J. K., Lehman, M. K., Nuxoll, A. S., Steinke, L., Sadykov, M., Powers,
793 R., & Fey, P. D. (2017). Amino Acid Catabolism in Staphylococcus aureus and the
794 Function of Carbon Catabolite Repression. *mBio*, *8*(1).
795 https://doi.org/10.1128/mBio.01434-16
796 Handa, N., Terada, T., Doi-Katayama, Y., Hirota, H., Tame, J. R., Park, S. Y., Kuramitsu, S.,
797 Shirouzu, M., & Yokoyama, S. (2005). Crystal structure of a novel polyisoprenoid-
798 binding protein from Thermus thermophilus HB8. *Protein Sci*, *14*(4), 1004-1010.
799 https://doi.org/10.1110/ps.041183305
800 Harper, L., Balasubramanian, D., Ohneck, E. A., Sause, W. E., Chapman, J., Mejia-Sosa, B.,
801 Lhakhang, T., Heguy, A., Tsirigos, A., Ueberheide, B., Boyd, J. M., Lun, D. S., & Torres, V.
802 J. (2018). Staphylococcus aureus Responds to the Central Metabolite Pyruvate To
803 Regulate Virulence. *mBio*, *9*(1). https://doi.org/10.1128/mBio.02272-17
804 Haupt, K., Reuter, M., van den Elsen, J., Burman, J., Hälbich, S., Richter, J., Skerka, C., &
805 Zipfel, P. F. (2008). The Staphylococcus aureus protein Sbi acts as a complement

806 inhibitor and forms a tripartite complex with host complement Factor H and C3b. *PLoS*
807 *Pathog*, *4*(12), e1000250. https://doi.org/10.1371/journal.ppat.1000250
808 Higgins, J., Loughman, A., van Kessel, K. P., van Strijp, J. A., & Foster, T. J. (2006). Clumping
809 factor A of Staphylococcus aureus inhibits phagocytosis by human
810 polymorphonuclear leucocytes. *FEMS Microbiol Lett*, *258*(2), 290-296.
811 https://doi.org/10.1111/j.1574-6968.2006.00229.x
812 Hines, K. M., Alvarado, G., Chen, X., Gatto, C., Pokorny, A., Alonzo, F., 3rd, Wilkinson, B. J., &
813 Xu, L. (2020). Lipidomic and Ultrastructural Characterization of the Cell Envelope of
814 Staphylococcus aureus Grown in the Presence of Human Serum. *mSphere*, *5*(3).
815 https://doi.org/10.1128/mSphere.00339-20
816 Hornef, M. W., Wick, M. J., Rhen, M., & Normark, S. (2002). Bacterial strategies for overcoming
817 host innate and adaptive immune responses. *Nat Immunol*, *3*(11), 1033-1040.
818 https://doi.org/10.1038/ni1102-1033
819 Horsburgh, M. J., Clements, M. O., Crossley, H., Ingham, E., & Foster, S. J. (2001). PerR
820 controls oxidative stress resistance and iron storage proteins and is required for
821 virulence in Staphylococcus aureus. *Infect Immun*, *69*(6), 3744-3754.
822 https://doi.org/10.1128/iai.69.6.3744-3754.2001
823 Howden, B. P., Giulieri, S. G., Wong Fok Lung, T., Baines, S. L., Sharkey, L. K., Lee, J. Y. H.,
824 Hachani, A., Monk, I. R., & Stinear, T. P. (2023). Staphylococcus aureus host
825 interactions and adaptation. *Nat Rev Microbiol*, *21*(6), 380-395.
826 https://doi.org/10.1038/s41579-023-00852-y
827 Imada, A., Nozaki, Y., Kawashima, F., & Yoneda, M. (1977). Regulation of glucosamine
828 utilization in Staphylococcus aureus and Escherichia coli. *J Gen Microbiol*, *100*(2),
829 329-337. https://doi.org/10.1099/00221287-100-2-329
830 Imlay, J. A. (2008). Cellular defenses against superoxide and hydrogen peroxide. *Annu Rev*
831 *Biochem*, *77*, 755-776. https://doi.org/10.1146/annurev.biochem.77.061606.161055
832 Ji, C. J., Kim, J. H., Won, Y. B., Lee, Y. E., Choi, T. W., Ju, S. Y., Youn, H., Helmann, J. D., & Lee,
833 J. W. (2015). Staphylococcus aureus PerR Is a Hypersensitive Hydrogen Peroxide
834 Sensor using Iron-mediated Histidine Oxidation. *J Biol Chem*, *290*(33), 20374-20386.
835 https://doi.org/10.1074/jbc.M115.664961
836 Jongerius, I., Garcia, B. L., Geisbrecht, B. V., van Strijp, J. A. G., & Rooijakkers, S. H. M. (2010).
837 Convertase inhibitory properties of Staphylococcal extracellular complement-binding
838 protein. *J Biol Chem*, *285*(20), 14973-14979. https://doi.org/10.1074/jbc.M109.091975
839 Joo, H. S., & Otto, M. (2015). Mechanisms of resistance to antimicrobial peptides in
840 staphylococci. *Biochim Biophys Acta*, *1848*(11 Pt B), 3055-3061.
841 https://doi.org/10.1016/j.bbamem.2015.02.009
842 Jorge, A. M., Schneider, J., Unsleber, S., Göhring, N., Mayer, C., & Peschel, A. (2017).
843 Utilization of glycerophosphodiesters by Staphylococcus aureus. *Mol Microbiol*,
844 *103*(2), 229-241. https://doi.org/10.1111/mmi.13552
845 Kenny, J. G., Moran, J., Kolar, S. L., Ulanov, A., Li, Z., Shaw, L. N., Josefsson, E., & Horsburgh,
846 M. J. (2013). Mannitol utilisation is required for protection of Staphylococcus aureus
847 from human skin antimicrobial fatty acids. *PLoS One*, *8*(7), e67698.
848 https://doi.org/10.1371/journal.pone.0067698
849 Kim, J., Kim, G. L., Norambuena, J., Boyd, J. M., & Parker, D. (2023). Impact of the pentose
850 phosphate pathway on metabolism and pathogenesis of Staphylococcus aureus.
851 *PLoS Pathog*, *19*(7), e1011531. https://doi.org/10.1371/journal.ppat.1011531
852 Kriegeskorte, A., Block, D., Drescher, M., Windmüller, N., Mellmann, A., Baum, C., Neumann,
853 C., Lorè, N. I., Bragonzi, A., Liebau, E., Hertel, P., Seggewiss, J., Becker, K., Proctor, R.
854 A., Peters, G., & Kahl, B. C. (2014). Inactivation of thyA in Staphylococcus aureus

855 attenuates virulence and has a strong impact on metabolism and virulence gene
856 expression. *mBio*, *5*(4), e01447-01414. https://doi.org/10.1128/mBio.01447-14
857 Kuehl, R., Morata, L., Meylan, S., Mensa, J., & Soriano, A. (2020). When antibiotics fail: a
858 clinical and microbiological perspective on antibiotic tolerance and persistence of
859 Staphylococcus aureus. *J Antimicrob Chemother*, *75*(5), 1071-1086.
860 https://doi.org/10.1093/jac/dkz559
861 Kwiecinski, J. M., & Horswill, A. R. (2020). Staphylococcus aureus bloodstream infections:
862 pathogenesis and regulatory mechanisms. *Curr Opin Microbiol*, *53*, 51-60.
863 https://doi.org/10.1016/j.mib.2020.02.005
864 Ledala, N., Zhang, B., Seravalli, J., Powers, R., & Somerville, G. A. (2014). Influence of iron and
865 aeration on Staphylococcus aureus growth, metabolism, and transcription. *J*
866 *Bacteriol*, *196*(12), 2178-2189. https://doi.org/10.1128/jb.01475-14
867 Ledger, E. V. K., Mesnage, S., & Edwards, A. M. (2022). Human serum triggers antibiotic
868 tolerance in Staphylococcus aureus. *Nat Commun*, *13*(1), 2041.
869 https://doi.org/10.1038/s41467-022-29717-3
870 Leibig, M., Liebeke, M., Mader, D., Lalk, M., Peschel, A., & Götz, F. (2011). Pyruvate formate
871 lyase acts as a formate supplier for metabolic processes during anaerobiosis in
872 Staphylococcus aureus. *J Bacteriol*, *193*(4), 952-962.
873 https://doi.org/10.1128/jb.01161-10
874 Lopatkin, A. J., Stokes, J. M., Zheng, E. J., Yang, J. H., Takahashi, M. K., You, L., & Collins, J. J.
875 (2019). Bacterial metabolic state more accurately predicts antibiotic lethality than
876 growth rate. *Nat Microbiol*, *4*(12), 2109-2117. https://doi.org/10.1038/s41564-019-
877 0536-0
878 Malachowa, N., Whitney, A. R., Kobayashi, S. D., Sturdevant, D. E., Kennedy, A. D.,
879 Braughton, K. R., Shabb, D. W., Diep, B. A., Chambers, H. F., Otto, M., & DeLeo, F. R.
880 (2011). Global changes in Staphylococcus aureus gene expression in human blood.
881 *PLoS One*, *6*(4), e18617. https://doi.org/10.1371/journal.pone.0018617
882 Mathelié-Guinlet, M., Viela, F., Alfeo, M. J., Pietrocola, G., Speziale, P., & Dufrêne, Y. F. (2020).
883 Single-Molecule Analysis Demonstrates Stress-Enhanced Binding between
884 Staphylococcus aureus Surface Protein IsdB and Host Cell Integrins. *Nano Lett*,
885 *20*(12), 8919-8925. https://doi.org/10.1021/acs.nanolett.0c04015
886 Mathew, J., Sankar, P., & Varacallo, M. (2023). Physiology, Blood Plasma. In *StatPearls*.
887 StatPearls Publishing
888 Copyright © 2023, StatPearls Publishing LLC.
889 Mu, A., Klare, W. P., Baines, S. L., Ignatius Pang, C. N., Guérillot, R., Harbison-Price, N.,
890 Keller, N., Wilksch, J., Nhu, N. T. K., Phan, M. D., Keller, B., Nijagal, B., Tull, D.,
891 Dayalan, S., Chua, H. H. C., Skoneczny, D., Koval, J., Hachani, A., Shah, A. Walker, M.
892 J. (2023). Integrative omics identifies conserved and pathogen-specific responses of
893 sepsis-causing bacteria. *Nat Commun*, *14*(1), 1530. https://doi.org/10.1038/s41467-
894 023-37200-w
895 Murdoch, C. C., & Skaar, E. P. (2022). Nutritional immunity: the battle for nutrient metals at
896 the host-pathogen interface. *Nat Rev Microbiol*, *20*(11), 657-670.
897 https://doi.org/10.1038/s41579-022-00745-6
898 Murphey, W. H., & Rosenblum, E. D. (1964). MANNITOL CATABOLISM BY STAPHYLOCOCCUS
899 AUREUS. *Arch Biochem Biophys*, *107*, 292-297. https://doi.org/10.1016/0003-
900 9861(64)90332-7
901 Murray, C. J., Ikuta, K. S., Sharara, F., Swetschinski, L., Aguilar, G. R., Gray, A., Han, C.,
902 Bisignano, C., Rao, P., & Wool, E. (2022). Global burden of bacterial antimicrobial
903 resistance in 2019: a systematic analysis. *The lancet*, *399*(10325), 629-655.

Njenga, R., Boele, J., Öztürk, Y., & Koch, H. G. (2023). Coping with stress: How bacteria fine-tune protein synthesis and protein transport. *J Biol Chem*, *299*(9), 105163. https://doi.org/10.1016/j.jbc.2023.105163

Nolan, A. C., Zeden, M. S., Kviatkovski, I., Campbell, C., Urwin, L., Corrigan, R. M., Gründling, A., & O'Gara, J. P. (2023). Purine Nucleosides Interfere with c-di-AMP Levels and Act as Adjuvants To Re-Sensitize MRSA To β-Lactam Antibiotics. *mBio*, *14*(1), e0247822. https://doi.org/10.1128/mbio.02478-22

O'Connor, M. J., Bartler, A. V., Ho, K. C., Zhang, K., Casas Fuentes, R. J., Melnick, B. A., Huffman, K. N., Hong, S. J., & Galiano, R. D. (2024). Understanding Staphylococcus aureus in hyperglycaemia: A review of virulence factor and metabolic adaptations. *Wound Repair Regen*, *32*(5), 661-670. https://doi.org/10.1111/wrr.13192

Overton, T. W., Justino, M. C., Li, Y., Baptista, J. M., Melo, A. M., Cole, J. A., & Saraiva, L. M. (2008). Widespread distribution in pathogenic bacteria of di-iron proteins that repair oxidative and nitrosative damage to iron-sulfur centers. *J Bacteriol*, *190*(6), 2004-2013. https://doi.org/10.1128/jb.01733-07

Paiva, T. O., Geoghegan, J. A., & Dufrêne, Y. F. (2023). High-force catch bonds between the Staphylococcus aureus surface protein SdrE and complement regulator factor H drive immune evasion. *Commun Biol*, *6*(1), 302. https://doi.org/10.1038/s42003-023-04660-1

Parsons, J. B., & Rock, C. O. (2013). Bacterial lipids: metabolism and membrane homeostasis. *Prog Lipid Res*, *52*(3), 249-276. https://doi.org/10.1016/j.plipres.2013.02.002

Pishchany, G., Sheldon, J. R., Dickson, C. F., Alam, M. T., Read, T. D., Gell, D. A., Heinrichs, D. E., & Skaar, E. P. (2014). IsdB-dependent hemoglobin binding is required for acquisition of heme by Staphylococcus aureus. *J Infect Dis*, *209*(11), 1764-1772. https://doi.org/10.1093/infdis/jit817

Potter, A. D., Butrico, C. E., Ford, C. A., Curry, J. M., Trenary, I. A., Tummarakota, S. S., Hendrix, A. S., Young, J. D., & Cassat, J. E. (2020). Host nutrient milieu drives an essential role for aspartate biosynthesis during invasive Staphylococcus aureus infection. *Proc Natl Acad Sci U S A*, *117*(22), 12394-12401. https://doi.org/10.1073/pnas.1922211117

Price, E. E., & Boyd, J. M. (2020). Genetic Regulation of Metal Ion Homeostasis in Staphylococcus aureus. *Trends Microbiol*, *28*(10), 821-831. https://doi.org/10.1016/j.tim.2020.04.004

Purves, J., Cockayne, A., Moody, P. C., & Morrissey, J. A. (2010). Comparison of the regulation, metabolic functions, and roles in virulence of the glyceraldehyde-3-phosphate dehydrogenase homologues gapA and gapB in Staphylococcus aureus. *Infect Immun*, *78*(12), 5223-5232. https://doi.org/10.1128/iai.00762-10

Qi, Z., Sun, N., & Liu, C. (2023). Glyoxylate cycle maintains the metabolic homeostasis of Pseudomonas aeruginosa in viable but nonculturable state induced by chlorine stress. *Microbiol Res*, *270*, 127341. https://doi.org/10.1016/j.micres.2023.127341

Rack, J. G., Morra, R., Barkauskaite, E., Kraehenbuehl, R., Ariza, A., Qu, Y., Ortmayer, M., Leidecker, O., Cameron, D. R., Matic, I., Peleg, A. Y., Leys, D., Traven, A., & Ahel, I. (2015). Identification of a Class of Protein ADP-Ribosylating Sirtuins in Microbial Pathogens. *Mol Cell*, *59*(2), 309-320. https://doi.org/10.1016/j.molcel.2015.06.013

Rack, J. G. M., Palazzo, L., & Ahel, I. (2020). (ADP-ribosyl)hydrolases: structure, function, and biology. *Genes Dev*, *34*(5-6), 263-284. https://doi.org/10.1101/gad.334631.119

Ramond, E., Gesbert, G., Rigard, M., Dairou, J., Dupuis, M., Dubail, I., Meibom, K., Henry, T., Barel, M., & Charbit, A. (2014). Glutamate utilization couples oxidative stress defense

953 and the tricarboxylic acid cycle in Francisella phagosomal escape. *PLoS Pathog*, *10*(1),
954 e1003893. https://doi.org/10.1371/journal.ppat.1003893
955 Räz, A. K., Andreoni, F., Boumasmoud, M., Bergada-Pijuan, J., Schweizer, T. A., Mairpady
956 Shambat, S., Hasse, B., Zinkernagel, A. S., & Brugger, S. D. (2023). Limited Adaptation
957 of Staphylococcus aureus during Transition from Colonization to Invasive Infection.
958 *Microbiol Spectr*, *11*(4), e0259021. https://doi.org/10.1128/spectrum.02590-21
959 Remy, L., Carrière, M., Derré-Bobillot, A., Martini, C., Sanguinetti, M., & Borezée-Durant, E.
960 (2013). The Staphylococcus aureus Opp1 ABC transporter imports nickel and cobalt in
961 zinc-depleted conditions and contributes to virulence. *Mol Microbiol*, *87*(4), 730-743.
962 https://doi.org/10.1111/mmi.12126
963 Richardson, A. R., Somerville, G. A., & Sonenshein, A. L. (2015). Regulating the Intersection of
964 Metabolism and Pathogenesis in Gram-positive Bacteria. *Microbiol Spectr*, *3*(3).
965 https://doi.org/10.1128/microbiolspec.MBP-0004-2014
966 Rohart, F., Gautier, B., Singh, A., & KA, L. C. (2017). mixOmics: An R package for 'omics
967 feature selection and multiple data integration. *PLoS Comput Biol*, *13*(11), e1005752.
968 https://doi.org/10.1371/journal.pcbi.1005752
969 Sachla, A. J., & Helmann, J. D. (2019). A bacterial checkpoint protein for ribosome assembly
970 moonlights as an essential metabolite-proofreading enzyme. *Nat Commun*, *10*(1),
971 1526. https://doi.org/10.1038/s41467-019-09508-z
972 Seo, K. S., Park, N., Rutter, J. K., Park, Y., Baker, C. L., Thornton, J. A., & Park, J. Y. (2021). Role
973 of Glucose-6-Phosphate in Metabolic Adaptation of Staphylococcus aureus in
974 Diabetes. *Microbiol Spectr*, *9*(2), e0085721. https://doi.org/10.1128/Spectrum.00857-
975 21
976 Sheldon, J. R., Marolda, C. L., & Heinrichs, D. E. (2014). TCA cycle activity in Staphylococcus
977 aureus is essential for iron-regulated synthesis of staphyloferrin A, but not
978 staphyloferrin B: the benefit of a second citrate synthase. *Mol Microbiol*, *92*(4), 824-
979 839. https://doi.org/10.1111/mmi.12593
980 Simon, G. M., & Cravatt, B. F. (2010). Activity-based proteomics of enzyme superfamilies:
981 serine hydrolases as a case study. *J Biol Chem*, *285*(15), 11051-11055.
982 https://doi.org/10.1074/jbc.R109.097600
983 Singh, A., Shannon, C. P., Gautier, B., Rohart, F., Vacher, M., Tebbutt, S. J., & KA, L. C. (2019).
984 DIABLO: an integrative approach for identifying key molecular drivers from multi-
985 omics assays. *Bioinformatics*, *35*(17), 3055-3062.
986 https://doi.org/10.1093/bioinformatics/bty1054
987 Smith, E. J., Visai, L., Kerrigan, S. W., Speziale, P., & Foster, T. J. (2011). The Sbi protein is a
988 multifunctional immune evasion factor of Staphylococcus aureus. *Infect Immun*,
989 *79*(9), 3801-3809. https://doi.org/10.1128/iai.05075-11
990 Soe, Y. M., Bedoui, S., Stinear, T. P., & Hachani, A. (2021). Intracellular Staphylococcus
991 aureus and host cell death pathways. *Cell Microbiol*, *23*(5), e13317.
992 https://doi.org/10.1111/cmi.13317
993 Spaan, A. N., Vrieling, M., Wallet, P., Badiou, C., Reyes-Robles, T., Ohneck, E. A., Benito, Y.,
994 de Haas, C. J., Day, C. J., Jennings, M. P., Lina, G., Vandenesch, F., van Kessel, K. P.,
995 Torres, V. J., van Strijp, J. A., & Henry, T. (2014). The staphylococcal toxins γ-
996 haemolysin AB and CB differentially target phagocytes by employing specific
997 chemokine receptors. *Nat Commun*, *5*, 5438. https://doi.org/10.1038/ncomms6438
998 Tavares, A. F., Teixeira, M., Romão, C. C., Seixas, J. D., Nobre, L. S., & Saraiva, L. M. (2011).
999 Reactive oxygen species mediate bactericidal killing elicited by carbon monoxide-
1000 releasing molecules. *J Biol Chem*, *286*(30), 26708-26717.
1001 https://doi.org/10.1074/jbc.M111.255752

1002 Toledano, M. B., Delaunay, A., Monceau, L., & Tacnet, F. (2004). Microbial H2O2 sensors as
1003 archetypical redox signaling modules. *Trends Biochem Sci*, *29*(7), 351-357.
1004 https://doi.org/10.1016/j.tibs.2004.05.005
1005 Tomlinson, K. L., Lung, T. W. F., Dach, F., Annavajhala, M. K., Gabryszewski, S. J., Groves, R.
1006 A., Drikic, M., Francoeur, N. J., Sridhar, S. H., Smith, M. L., Khanal, S., Britto, C. J.,
1007 Sebra, R., Lewis, I., Uhlemann, A. C., Kahl, B. C., Prince, A. S., & Riquelme, S. A. (2021).
1008 Staphylococcus aureus induces an itaconate-dominated immunometabolic response
1009 that drives biofilm formation. *Nat Commun*, *12*(1), 1399.
1010 https://doi.org/10.1038/s41467-021-21718-y
1011 Tomlinson, K. L., & Riquelme, S. A. (2021). Host-bacteria metabolic crosstalk drives S. aureus
1012 biofilm. *Microb Cell*, *8*(5), 106-107. https://doi.org/10.15698/mic2021.05.749
1013 Wick, R. R., Judd, L. M., Cerdeira, L. T., Hawkey, J., Méric, G., Vezina, B., Wyres, K. L., & Holt,
1014 K. E. (2021). Trycycler: consensus long-read assemblies for bacterial genomes.
1015 *Genome Biol*, *22*(1), 266. https://doi.org/10.1186/s13059-021-02483-z
1016 Wolff, D. W., Deng, Z., Bianchi-Smiraglia, A., Foley, C. E., Han, Z., Wang, X., Shen, S.,
1017 Rosenberg, M. M., Moparthy, S., Yun, D. H., Chen, J., Baker, B. K., Roll, M. V., Magiera,
1018 A. J., Li, J., Hurley, E., Feltri, M. L., Cox, A. Nikiforov, M. A. (2022). Phosphorylation of
1019 guanosine monophosphate reductase triggers a GTP-dependent switch from pro- to
1020 anti-oncogenic function of EPHA4. *Cell Chem Biol*, *29*(6), 970-984.e976.
1021 https://doi.org/10.1016/j.chembiol.2022.01.007
1022 Yan, J., Han, D., Liu, C., Gao, Y., Li, D., Liu, Y., & Yang, G. (2017). Staphylococcus aureus VraX
1023 specifically inhibits the classical pathway of complement by binding to C1q. *Mol*
1024 *Immunol*, *88*, 38-44. https://doi.org/10.1016/j.molimm.2017.05.018
1025 Yee, R., Cui, P., Shi, W., Feng, J., & Zhang, Y. (2015). Genetic Screen Reveals the Role of
1026 Purine Metabolism in Staphylococcus aureus Persistence to Rifampicin. *Antibiotics*
1027 *(Basel)*, *4*(4), 627-642. https://doi.org/10.3390/antibiotics4040627
1028 Yee, R., Feng, J., Wang, J., Chen, J., & Zhang, Y. (2019). Identification of Genes Regulating Cell
1029 Death in Staphylococcus aureus. *Front Microbiol*, *10*, 2199.
1030 https://doi.org/10.3389/fmicb.2019.02199
1031 Zhang, W., Zhang, M., Gao, C., Zhang, Y., Ge, Y., Guo, S., Guo, X., Zhou, Z., Liu, Q., Zhang, Y.,
1032 Ma, C., Tao, F., & Xu, P. (2017). Coupling between d-3-phosphoglycerate
1033 dehydrogenase and d-2-hydroxyglutarate dehydrogenase drives bacterial l-serine
1034 synthesis. *Proc Natl Acad Sci U S A*, *114*(36), E7574-e7582.
1035 https://doi.org/10.1073/pnas.1619034114
1036 Zhao, Y., van Kessel, K. P. M., de Haas, C. J. C., Rogers, M. R. C., van Strijp, J. A. G., & Haas, P.
1037 A. (2018). Staphylococcal superantigen-like protein 13 activates neutrophils via formyl
1038 peptide receptor 2. *Cell Microbiol*, *20*(11), e12941. https://doi.org/10.1111/cmi.12941
1039

1040

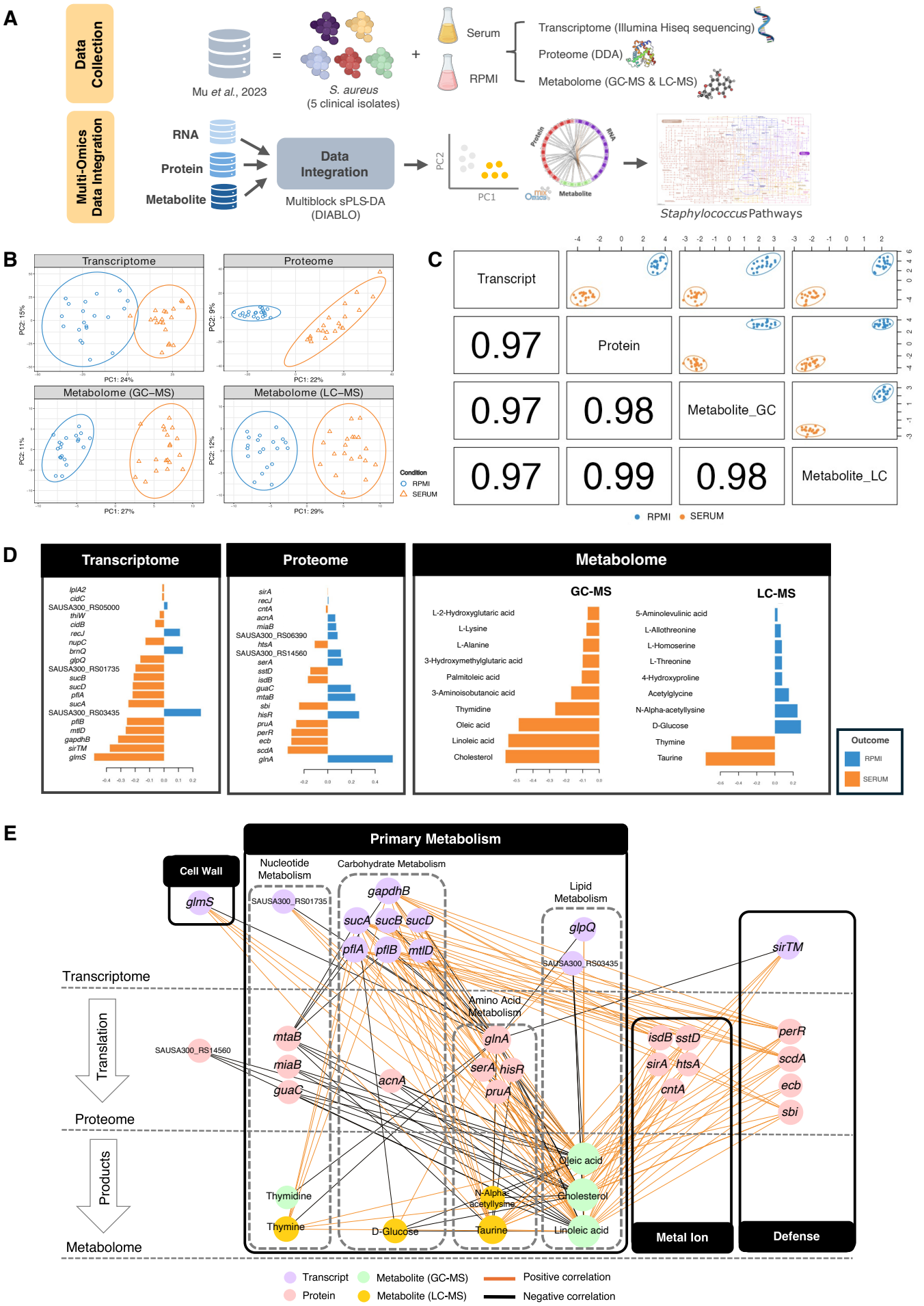
A
Data Collection
Mu et al., 2023
S. aureus
(5 clinical isolates)
Serum
RPMI
Transcriptome (Illumina Hiseq sequencing)
Proteome (DDA)
Metabolome (GC-MS & LC-MS)
Multi-Omics Data Integration
RNA
Protein
Metabolite
Data Integration
Multiblock sPLS-DA
(DIABLO)
PC2
PC1
Staphylococcus Pathways
B
Transcriptome
Proteome
Metabolome (GC–MS)
Metabolome (LC–MS)
PC1: 24%
PC2: 15%
PC1: 22%
PC2: 9%
PC1: 27%
PC2: 11%
PC1: 29%
PC2: 12%
Condition
RPMI
SERUM
C
Transcript
Protein
Metabolite_GC
Metabolite_LC
0.97
0.97
0.98
0.97
0.99
0.98
RPMI
SERUM
D
Transcriptome
Proteome
Metabolome
GC-MS
LC-MS
lplA2
cidC
SAUSA300_RS05000
thiW
cidB
recJ
nupC
brnQ
glpQ
SAUSA300_RS01735
sucB
sucD
pflA
sucA
SAUSA300_RS03435
pflB
mtlD
gapdhB
sirTM
glmS
sirA
recJ
cntA
acnA
miaB
SAUSA300_RS06390
htsA
SAUSA300_RS14560
serA
sstD
isdB
guaC
mtaB
sbi
hisR
pruA
perR
ecb
scdA
glnA
L-2-Hydroxyglutaric acid
L-Lysine
L-Alanine
3-Hydroxymethylglutaric acid
Palmitoleic acid
3-Aminoisobutanoic acid
Thymidine
Oleic acid
Linoleic acid
Cholesterol
5-Aminolevulinic acid
L-Allothreonine
L-Homoserine
L-Threonine
4-Hydroxyproline
Acetylglycine
N-Alpha-acetyllysine
D-Glucose
Thymine
Taurine
Outcome
RPMI
SERUM
E
Primary Metabolism
Cell Wall
glmS
Nucleotide Metabolism
SAUSA300_RS01735
Carbohydrate Metabolism
gapdhB
sucA sucB sucD
pflA pflB mtlD
Lipid Metabolism
glpQ
SAUSA300_RS03435
Amino Acid Metabolism
glnA
serA hisR
pruA
SAUSA300_RS14560
mtaB
miaB
guaC
acnA
Thymidine
Thymine
D-Glucose
N-Alpha-acetyllysine
Taurine
Oleic acid
Cholesterol
Linoleic acid
isdB sstD
sirA htsA
cntA
Metal Ion
sirTM
perR
scdA
ecb
sbi
Defense
Transcriptome
Translation
Proteome
Products
Metabolome
Transcript
Protein
Metabolite (GC-MS)
Metabolite (LC-MS)
Positive correlation
Negative correlation

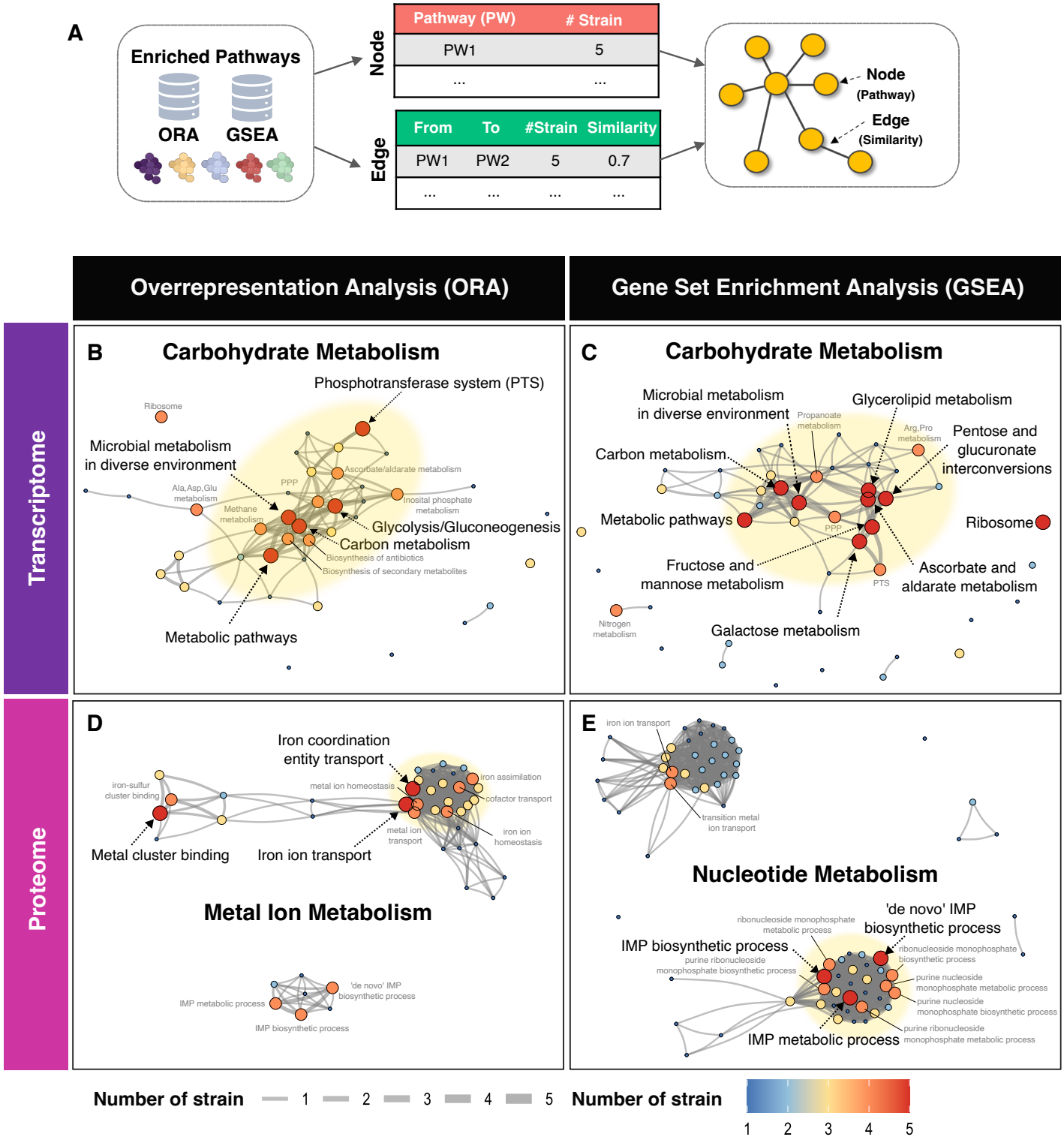
A
Enriched Pathways
ORA
GSEA
Node
Pathway (PW)
Strain
PW1
5
...
...
Edge
From
To
#Strain
Similarity
PW1
PW2
5
0.7
...
...
...
...
Node
(Pathway)
Edge
(Similarity)
Overrepresentation Analysis (ORA)
Gene Set Enrichment Analysis (GSEA)
Transcriptome
Proteome
B
Carbohydrate Metabolism
Phosphotransferase system (PTS)
Ribosome
Microbial metabolism
in diverse environment
Ala,Asp,Glu
metabolism
PPP
Ascorbate/aldarate metabolism
Methane
metabolism
Inosital phosphate
metabolism
Glycolysis/Gluconeogenesis
Carbon metabolism
Biosynthesis of antibiotics
Biosynthesis of secondary metabolites
Metabolic pathways
C
Carbohydrate Metabolism
Microbial metabolism
in diverse environment
Glycerolipid metabolism
Propanoate
metabolism
Arg,Pro
metabolism
Pentose and
glucuronate
interconversions
Carbon metabolism
Metabolic pathways
PPP
Ribosome
Fructose and
mannose metabolism
PTS
Ascorbate and
aldarate metabolism
Nitrogen
metabolism
Galactose metabolism
D
Iron coordination
entity transport
iron-sulfur
cluster binding
metal ion homeostasis
iron assimilation
cofactor transport
metal ion
transport
iron ion
homeostasis
Metal cluster binding
Iron ion transport
Metal Ion Metabolism
IMP metabolic process
'de novo' IMP
biosynthetic process
IMP biosynthetic process
E
iron ion transport
transition metal
ion transport
Nucleotide Metabolism
ribonucleoside monophosphate
metabolic process
'de novo' IMP
biosynthetic process
IMP biosynthetic process
purine ribonucleoside
monophosphate biosynthetic process
ribonucleoside monophosphate
biosynthetic process
purine nucleoside
monophosphate metabolic process
purine nucleoside
monophosphate biosynthetic process
purine ribonucleoside
monophosphate metabolic process
IMP metabolic process
Number of strain
1
2
3
4
5
Number of strain
1
2
3
4
5

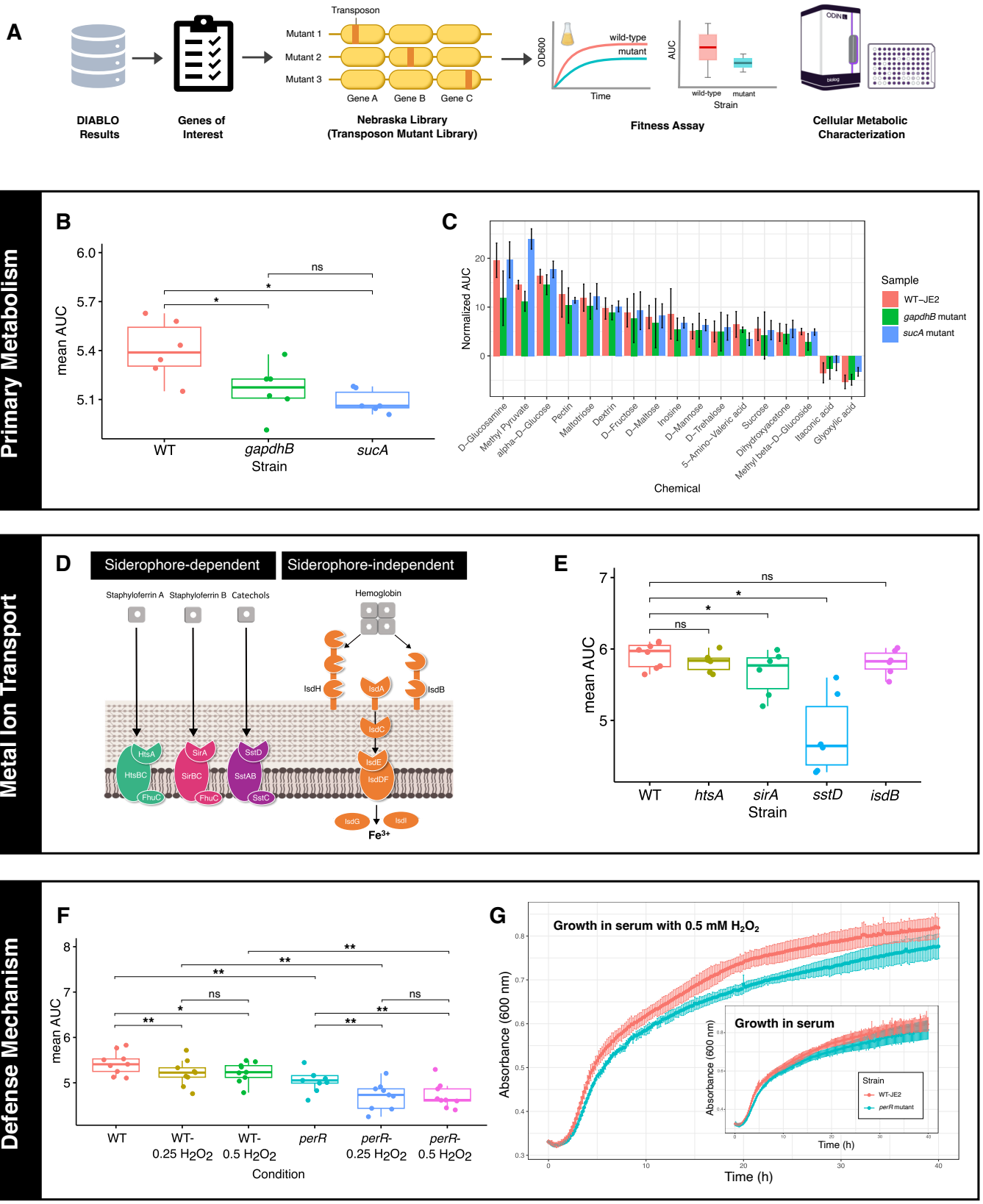
A
DIABLO Results
Genes of Interest
Transposon
Mutant 1
Mutant 2
Mutant 3
Gene A
Gene B
Gene C
Nebraska Library (Transposon Mutant Library)
OD600
wild-type
mutant
Time
AUC
wild-type
mutant
Strain
Fitness Assay
Cellular Metabolic Characterization
Primary Metabolism
B
mean AUC
ns
*
*
WT
gapdhB
sucA
Strain
C
Normalized AUC
Sample
WT–JE2
gapdhB mutant
sucA mutant
D-Glucosamine
Methyl Pyruvate
alpha-D-Glucose
Pectin
Maltotriose
Dextrin
D-Fructose
D-Maltose
Inosine
D-Mannose
D-Trehalose
5-Amino-Valeric acid
Sucrose
Dihydroxyacetone
Methyl beta-D-Glucoside
Itaconic acid
Glyoxylic acid
Chemical
Metal Ion Transport
D
Siderophore-dependent
Siderophore-independent
Staphyloferrin A
Staphyloferrin B
Catechols
Hemoglobin
IsdH
IsdA
IsdB
IsdC
IsdE
IsdDF
IsdG
IsdI
HtsA
HtsBC
FhuC
SirA
SirBC
FhuC
SstD
SstAB
SstC
Fe3+
E
mean AUC
ns
*
*
ns
WT
htsA
sirA
sstD
isdB
Strain
Defense Mechanism
F
mean AUC
**
**
**
ns
*
**
ns
**
**
WT
WT-0.25 H2O2
WT-0.5 H2O2
perR
perR-0.25 H2O2
perR-0.5 H2O2
Condition
G
Growth in serum with 0.5 mM H2O2
Absorbance (600 nm)
Time (h)
Growth in serum
Strain
WT-JE2
perR mutant

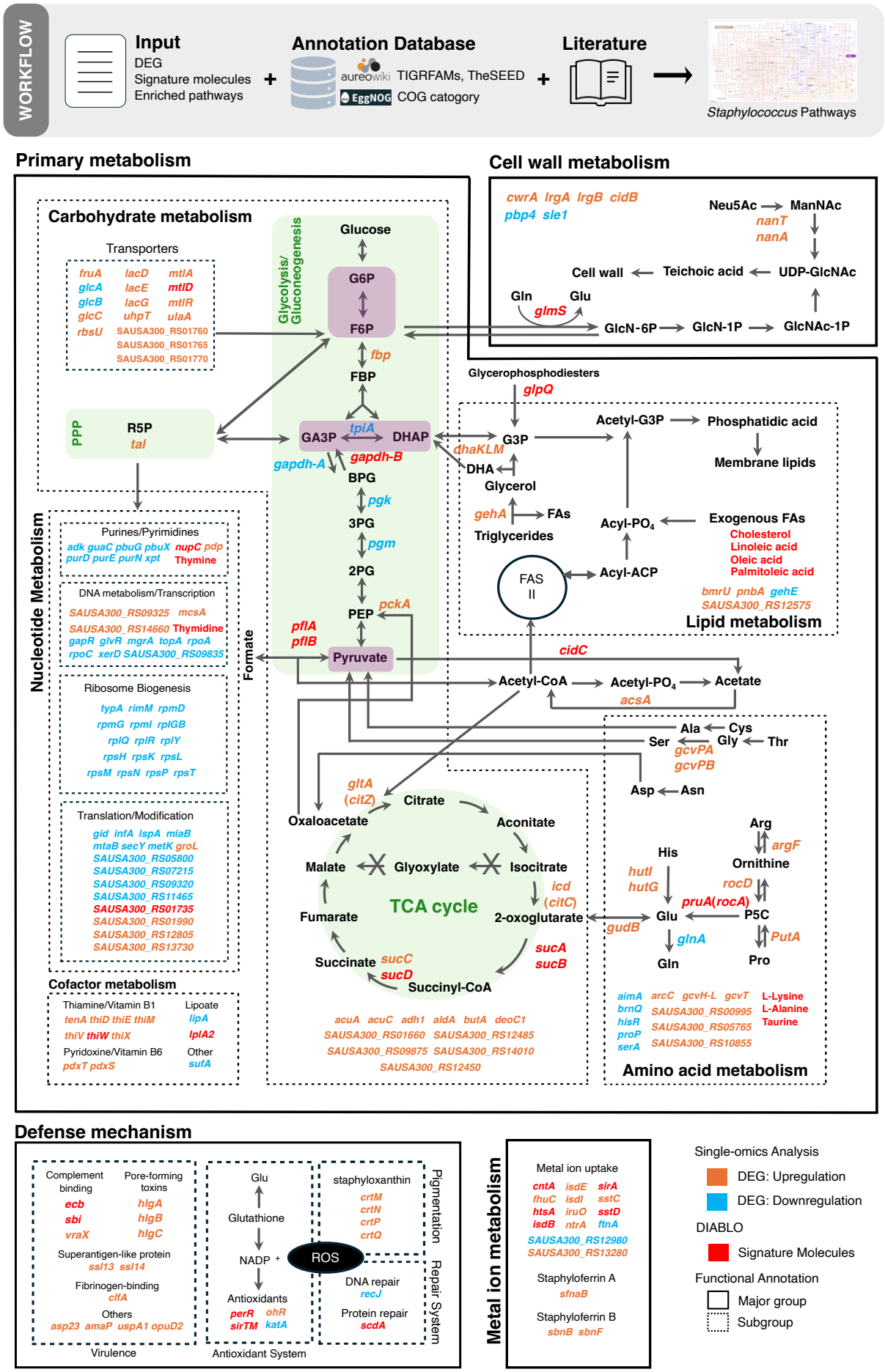
WORKFLOW
Input
DEG
Signature molecules
Enriched pathways
Annotation Database
aureowiki TIGRFAMs, TheSEED
EggNOG COG catogory
Literature
Staphylococcus Pathways
Primary metabolism
Carbohydrate metabolism
Transporters
fruA lacD mtlA
glcA lacE mtlD
glcB lacG mtlR
glcC uhpT ulaA
rbsU SAUSA300_RS01760
SAUSA300_RS01765
SAUSA300_RS01770
Glycolysis/ Gluconeogenesis
Glucose
G6P
F6P
fbp
FBP
PPP
R5P
tal
GA3P
tpiA
DHAP
gapdh-A
gapdh-B
BPG
pgk
3PG
pgm
2PG
PEP
pckA
pflA
pflB
Pyruvate
Formate
Nucleotide Metabolism
Purines/Pyrimidines
adk guaC pbuG pbuX nupC pdp
purD purE purN xpt Thymine
DNA metabolism/Transcription
SAUSA300_RS09325 mcsA
SAUSA300_RS14660 Thymidine
gapR glvR mgrA topA rpoA
rpoC xerD SAUSA300_RS09835
Ribosome Biogenesis
typA rimM rpmD
rpmG rpmI rplGB
rplQ rplR rplY
rpsH rpsK rpsL
rpsM rpsN rpsP rpsT
Translation/Modification
gid infA lspA miaB
mtaB secY metK groL
SAUSA300_RS05800
SAUSA300_RS07215
SAUSA300_RS09320
SAUSA300_RS11465
SAUSA300_RS01735
SAUSA300_RS01990
SAUSA300_RS12805
SAUSA300_RS13730
Cofactor metabolism
Thiamine/Vitamin B1
tenA thiD thiE thiM
thiV thiW thiX
Pyridoxine/Vitamin B6
pdxT pdxS
Lipoate
lipA
lplA2
Other
sufA
Cell wall metabolism
cwrA lrgA lrgB cidB
pbp4 sle1
Neu5Ac
ManNAc
nanT
nanA
Cell wall
Teichoic acid
UDP-GlcNAc
Gln
Glu
glmS
GlcN-6P
GlcN-1P
GlcNAc-1P
Glycerophosphodiesters
glpQ
G3P
dhaKLM
DHA
Glycerol
Acetyl-G3P
Phosphatidic acid
Membrane lipids
gehA
FAs
Triglycerides
Acyl-PO4
Exogenous FAs
Cholesterol
Linoleic acid
Oleic acid
Palmitoleic acid
FAS II
Acyl-ACP
bmrU pnbA gehE
SAUSA300_RS12575
Lipid metabolism
cidC
Acetyl-CoA
Acetyl-PO4
Acetate
acsA
Ala
Cys
Ser
Gly
Thr
gcvPA
gcvPB
Asp
Asn
gltA (citZ)
Citrate
Oxaloacetate
Aconitate
Malate
Glyoxylate
Isocitrate
icd (citC)
TCA cycle
Fumarate
2-oxoglutarate
sucA
sucB
Succinate
sucC
sucD
Succinyl-CoA
acuA acuC adh1 aldA butA deoC1
SAUSA300_RS01660 SAUSA300_RS12485
SAUSA300_RS09875 SAUSA300_RS14010
SAUSA300_RS12450
Arg
argF
Ornithine
His
hutI
hutG
rocD
pruA(rocA)
Glu
P5C
gudB
glnA
PutA
Gln
Pro
aimA arcC gcvH-L gcvT
brnQ SAUSA300_RS00995
hisR SAUSA300_RS05765
proP SAUSA300_RS10855
serA
L-Lysine
L-Alanine
Taurine
Amino acid metabolism
Defense mechanism
Complement binding
ecb
sbi
vraX
Pore-forming toxins
hlgA
hlgB
hlgC
Superantigen-like protein
ssl13 ssl14
Fibrinogen-binding
clfA
Others
asp23 amaP uspA1 opuD2
Virulence
Glu
Glutathione
NADP +
ROS
Antioxidants
perR ohR
sirTM katA
Antioxidant System
staphyloxanthin
crtM
crtN
crtP
crtQ
Pigmentation
DNA repair
recJ
Protein repair
scdA
Repair System
Metal ion metabolism
Metal ion uptake
cntA isdE sirA
fhuC isdI sstC
htsA iruO sstD
isdB ntrA ftnA
SAUSA300_RS12980
SAUSA300_RS13280
Staphyloferrin A
sfnaB
Staphyloferrin B
sbnB sbnF
Single-omics Analysis
DEG: Upregulation
DEG: Downregulation
DIABLO
Signature Molecules
Functional Annotation
Major group
Subgroup